

The SOLRAD 10 Satellite, Explorer 44, 1971-058A

DONALD M. HORAN AND ROBERT W. KREPLIN

*Upper Air Physics Branch
Space Science Division*

July 12, 1972



PLEASE RETURN THIS COPY TO:

**NAVAL RESEARCH LABORATORY
WASHINGTON, D.C. 20375
ATTN: CODE 2628**

Because of our limited supply you are requested to return this copy as soon as it has served your purposes so that it may be made available to others for reference use. Your cooperation will be appreciated.

NDW-NRL-5070/2035 (Rev. 3-73)

**NAVAL RESEARCH LABORATORY
Washington, D.C.**

CONTENTS

| | |
|--|-----|
| Abstract | iii |
| Problem Status | iii |
| Authorization | iii |
| INTRODUCTION | 1 |
| THE EXPERIMENTS | 3 |
| General Information | 3 |
| Experiment 1: 0.5 to 3 Å Band | 3 |
| Experiment 2: 1 to 5 Å Band | 6 |
| Experiment 3: 1 to 8 Å Band | 7 |
| Experiment 4: 8 to 16 Å Band | 7 |
| Experiment 5: 1 to 20 Å Band, 44 to 60 Å Bands | 7 |
| Experiment 6: 1 to 20 Å Band | 8 |
| Experiment 7A: Lyman-Alpha Flare Detector | 8 |
| Experiment 7B: 1080 to 1350 Å Band | 8 |
| Experiment 8: 1225 to 1350 Å Band | 8 |
| Experiment 9: 1450 to 1600 Å Band | 9 |
| Experiment 10: Charged Particle Indicators | 9 |
| Experiment 11: 15 to 150 keV | 9 |
| Experiment 12: 170 to 700 Å Band | 9 |
| Experiment 13: 0.1 to 1.6 Å Band | 10 |
| Experiment 14: Satellite Temperature Monitor | 10 |
| Stellar X-Ray (Stellrad) Experiment | 10 |
| Protection from Trapped Charged Particles | 11 |
| EXPERIMENT ELECTRONICS | 12 |
| Electrometer-Amplifier Range Changes | 12 |
| Electrometer-Amplifier Calibration Sequence | 14 |
| DATA TRANSMISSION | 15 |
| Telemetry Systems | 15 |
| Primary Real-Time Data Transmission — PCM | 16 |
| Secondary Real-Time Data Transmission — Analog | 17 |
| Stored Data Transmission — Memory Data | 18 |
| Stellrad Data Transmission | 22 |
| DATA REDUCTION | 22 |
| X-Ray Experiments | 22 |
| Ultraviolet Experiments | 33 |
| Extreme Ultraviolet Experiment | 36 |

| | |
|--|----|
| SATELLITE ORIENTATION CONTROL | 38 |
| Spin and Attitude Control Systems | 38 |
| Aspect Sensor Data Transmission | 39 |
| ACKNOWLEDGMENTS | 40 |
| REFERENCES | 40 |
| APPENDIX A — Correction of Experiment 5 Data for Radiation with Wavelength Less than 20 Å | 41 |
| APPENDIX B — Substituting Temperature-Dependent, Bremsstrahlung-Type Spectra for Graybody Spectra | 44 |

ABSTRACT

The Naval Research Laboratory's SOLRAD 10 satellite, also known as Explorer 44 or 1971-058A, was launched on July 8, 1971. The satellite is equipped with sensors to measure solar x-ray and ultraviolet radiation in the following bands: 15 to 150 keV, 0.1 to 1.6 Å, 0.5 to 3 Å, 1 to 5 Å, 1 to 8 Å, 8 to 16 Å, 1 to 20 Å, 44 to 60 Å, 170 to 700 Å, 1080 to 1350 Å, 1225 to 1350 Å, and 1450 to 1600 Å. It also carries an experiment designed to search for radiation in the 0.5 to 15 Å band from nonsolar sources. The satellite is equipped with a data storage system which can accept data from almost all solar experiments with a 1-minute or a 3-minute resolution.

The satellite continuously transmits data in real-time at 137.710 MHz. Individual scientists and institutions have been invited through COSPAR to receive and use the data transmitted in real time in their own research programs. To encourage this participation, IRIG channel 7 carries data and status information for almost every solar experiment.

The experiment complement aboard SOLRAD 10 is described in detail, and the information needed to convert the telemetered data to solar flux values is provided.

PROBLEM STATUS

This is an interim report on one phase of the problem; work is continuing on other phases.

AUTHORIZATION

NRL Problem A01-20
Project A3705381-652B-2F00-551-771

Manuscript submitted March 7, 1972.

THE SOLRAD 10 SATELLITE
EXPLORER 44
1971-058A

INTRODUCTION

The Naval Research Laboratory's SOLRAD 10 satellite is the most recent of a series of eight successful satellites which began with the launch of SOLRAD 1 (1960 — Eta 2) on June 22, 1960. These satellites were launched to make continuous measurements of the sun's emission in the x-ray band. The last four satellites in the series have been highly successful — SOLRAD 7A (1964-01D), SOLRAD 7B (1965-16D), SOLRAD 8 (1965-93A), and SOLRAD 9 (1968-17A). With these spacecraft, solar x-ray radiation has been monitored since January 1964. During this period, the minimum and maximum x-ray flux levels of the current sunspot cycle have been determined, and solar x-ray emission has been observed in two or more x-ray bands throughout the increasing phase of this cycle and into the decreasing phase.

The data from satellites prior to SOLRAD 8 were transmitted only in real time and so could be recorded only when the satellites were within range of a ground station. SOLRAD 8 carried a data-storage system, but it operated for only a month. However, the satellite continued transmitting in real time and provided almost 2 years of reliable solar monitoring. SOLRAD 9 also contains a data-storage system, and this system has operated flawlessly for over 4 years to provide a nearly continuous record of solar activity since March 1968. SOLRAD 9 continues to transmit both real-time and stored data.

SOLRAD 10 (1971-058A) was launched by a NASA Scout rocket from Wallops Island, Virginia, at 2258 UT on July 8, 1971. Its orbit has a 51.0° inclination, a 340 naut mi apogee, a 235-naut mi perigee, and a 95.3-minute period. The 262-lb satellite (Fig. 1) is shaped like a 12-sided drum, 23 inches high and 30 inches in diameter across the corners. It differs from its immediate predecessors in that its spin axis is oriented toward the sun instead of perpendicular to the satellite-sun line. All of its solar experiment sensors are located on the aft end (as launched) of the satellite and aligned parallel to the spin axis. The sensors for a stellar experiment are located on the side of the satellite and aligned perpendicular to the spin axis. The four symmetrically mounted solar-cell panels, which resemble windmill blades, also serve as the four elements of the turnstile antenna system.

Individual scientists and institutions have been invited through COSPAR to receive and use the x-ray data in their own programs of research. One of the purposes of this report is to provide all information necessary for the reduction of the data transmitted in real time. Orbital elements and equator-crossing data are available from NASA, but requests for such information should be made to Code 7125, Naval Research Laboratory, Washington, D.C. 20390. Information concerning the status of the experiments and satellite will be kept current by publication in the Spacewarn Bulletin.

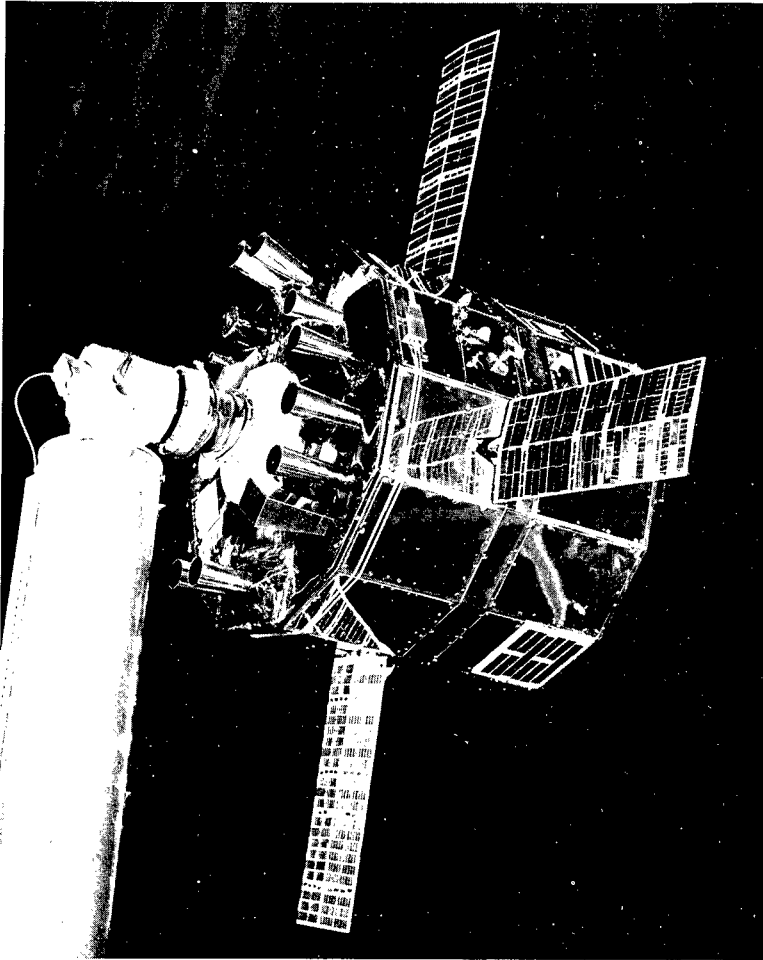


Fig. 1 — SOLRAD 10 during testing in the anechoic chamber. The satellite is basically a 12-sided drum, 23 inches high and 30 inches in diameter across the corners. The cones are aluminum collimators which protect some of the solar experiments from charged particles. The Stellrad sensor can be partially seen on the uppermost visible side panel. The solar panels also serve as elements of the antenna system.

THE EXPERIMENTS

General Information

The SOLRAD 10 solar experiments were selected to measure solar radiation in eight x-ray and five ultraviolet bands. The selected bands were chosen because of their utility in providing information on fundamental solar processes, prior experience with the bands, and sensitivity of various ionospheric layers to radiation within these bands. The following list identifies the bands selected for monitoring by solar experiments aboard SOLRAD 10:

| X-Ray | Ultraviolet |
|--------------|---------------|
| 15 — 150 keV | 170 — 500 Å |
| 0.1 — 1.6 Å | 170 — 700 Å |
| 0.5 — 3 Å | 1080 — 1350 Å |
| 1 — 5 Å | 1225 — 1350 Å |
| 1 — 8 Å | 1450 — 1600 Å |
| 8 — 16 Å | |
| 1 — 20 Å | |
| 44 — 60 Å | |

The dynamic ranges selected for each experiment are based on flux level variations observed by SOLRAD 9 and the expected decrease in solar x-ray emission during the waning phase of the current solar cycle. Detailed detector and amplifier information can be found in Table 1 and Table 2. Figure 2 shows the location of the experiments on the solar-oriented surface of SOLRAD 10.

In addition to the solar experiments, SOLRAD 10 carries an experiment to measure x-ray emission from stellar sources and a simple resistive-wire experiment to measure the temperature range encountered on the surface of SOLRAD 10 which is always turned away from the sun.

Experiment 1: 0.5 to 3 Å

Two independent ionization chambers sensitive to the 0.5 to 3 Å band of the x-ray spectrum are designated 1A and 1B. For redundancy, each ionization chamber is connected to its own four-range electrometer-amplifier and fed from a different power converter. The detector used for experiment 1A has a cylindrical chamber and uses a central pin and a metal mesh lining the chamber wall as electrodes. It is identical to the 0.5 to 3 Å ionization chamber used on SOLRAD 9 (Ref. 1). The ionization chamber used for experiment 1B is rectangular in cross section. Three parallel plates, which divide the chamber into four equal sections, serve as electrodes. The window area of the 1B detector is approximately a factor of three greater than that of the 1A detector. A ground command determines whether 1A or 1B will be connected to the telemetry and data-storage systems.

Table 1
SOLRAD 10 Solar Sensors

| Experiment Number | Band (angstroms) | Detector Type and Serial Number | Window Material and Thickness | $\rho x(W)$ (g/cm ²) | Filling Gas and Pressure* | Gas Filter Thickness (cm)† | $\rho x(G)$ (g/cm ²) | $\rho x(G)$ (g/cm ²)‡ | ω (ion pair/erg) | Effective Window Area (cm ²)# |
|-------------------|------------------|--|---|--|---------------------------|----------------------------|--|--|-------------------------|---|
| 1 A | 0.5 - 3 | Ion chamber 1281 | Beryllium 0.127 cm Aluminum 1000 A | 0.2472 2.7×10^{-5} | Kr 1520 | 0.094 | 7.0×10^{-4} | 1.89×10^{-2} | 2.57×10^{10} | 5.28 |
| 1 B | 0.5 - 3 | Ion chamber PP-3 | Beryllium 0.127 cm Aluminum 1000 A | 0.2299 2.7×10^{-5} | Kr 1520 | 0.112 | 8.3×10^{-4} | 1.89×10^{-2} | 2.57×10^{10} | 16.17 |
| 2 | 1 - 5 | Ion chamber 1313 | Beryllium 0.051 cm Aluminum 1000 A | 0.1003 2.7×10^{-5} | Ar 760 | 0.094 | 1.7×10^{-4} | 4.52×10^{-3} | 2.38×10^{10} | 5.28 |
| 3 A | 1 - 8 | Ion chamber 1302 | Beryllium 0.0127 cm Aluminum 1000 A | 0.0263 2.7×10^{-5} | Ar 760 | 0.094 | 1.7×10^{-4} | 4.52×10^{-3} | 2.38×10^{10} | 2.97 |
| 3 B | 1 - 8 | Ion chamber 1296 | Beryllium 0.0127 cm Aluminum 1000 A | 0.0249 2.7×10^{-5} | Ar 760 | 0.094 | 1.7×10^{-4} | 4.52×10^{-3} | 2.38×10^{10} | 2.97 |
| 4 A | 8 - 16 | Ion chamber 1316 | Aluminum 0.00085 cm | 2.44×10^{-3} | N ₂ 400 | 0.216 | 1.42×10^{-4} | 1.67×10^{-3} | 1.80×10^{10} | 1.12 |
| 4 B | 8 - 16 | Ion chamber 1319 | Aluminum 0.00085 cm | 2.44×10^{-3} | N ₂ 400 | 0.216 | 1.42×10^{-4} | 1.67×10^{-3} | 1.80×10^{10} | 0.40 |
| 5 | 1 - 20, 44 - 60 | Ion chamber 1342 | Mylar 0.00064 cm | 8.5×10^{-4} | N ₂ 170 | 0.216 | 6.05×10^{-5} | 7.1×10^{-4} | 1.80×10^{10} | 0.17 |
| 6 | 1 - 20 | Ion chamber 1331 | Mylar 0.00064 cm Aluminum 2500 A | 8.5×10^{-4} 6.3×10^{-5} | CCl ₄ 27 | 0.216 | 5.27×10^{-5} | 6.19×10^{-4} | 2.13×10^{10} | 0.17 |
| 7 A | 1080 - 1350 | Ion chamber CT-2 | Lithium fluoride | — | NO 20 | — | Quantum efficiency 38% at 1216 A | | | 2.68×10^{-3} |
| 7 B | 1080 - 1350 | Ion chamber M2208 M2209 | Lithium fluoride | — | NO 20 | — | Quantum efficiency 52% at 1216 A | | | 1.57×10^{-4} |
| 8 | 1225 - 1350 | Ion chamber M2259 M2266 | Calcium fluoride | — | NO 20 | — | Quantum efficiency assumed to average 25% over 1225 - 1350 A band. | | | 3.58×10^{-4} |
| 9 | 1450 - 1600 | Ion chamber M2317 M2318 | Silicon dioxide | — | Triethylamine 8 | — | Quantum efficiency assumed to average 10% over 1450 - 1600 A band. | | | 1.61×10^{-4} |
| 10 A | 0.5 - 3 | Ion chamber 1280 | Beryllium 0.127 cm Aluminum 1000 A | 0.2464 2.7×10^{-5} | Kr 1520 | 0.094 | 7.0×10^{-4} | 1.89×10^{-2} | 2.57×10^{10} | 5.28 |
| 10 B | 1 - 8 | Ion chamber 1295 | Beryllium 0.0127 cm Aluminum 1000 A | 0.0245 2.7×10^{-5} | Ar 760 | 0.094 | 1.7×10^{-4} | 4.52×10^{-3} | 2.38×10^{10} | 2.97 |
| 11 | 0.08 - 0.8 | CsI(Na) scintillating crystal (1 cm thick) | Mylar 0.05 cm Aluminum 0.05 cm Beryllium 0.01 Titanium Dioxide 0.03 cm Polyvinyltoluene 0.13 cm | — — — — — | — — — — — | — — — — — | — — — — — | — — — — — | — — — — — | 10.0 — — — — |
| 12 A | 170 - 500 | LiF photo sensitive surface 600-060-19 | Aluminum 2200 A Al ₂ O ₃ 160 A, Carbon 540 A | — | Vacuum | — | — | — | — | 1.93 |
| 12 B | 170 - 700 | LiF photo sensitive surface 600-060-16 | Aluminum 2200 A Al ₂ O ₃ 160 A | — | Vacuum | — | — | — | — | 0.079 |
| 13 | 0.1 - 1.6 | Ion chamber 12 | Beryllium 0.508 cm Aluminum 0.0254 cm | 0.955 0.0357 | Kr 912 Xe 228 | 0.318 | 1.30×10^{-3} 5.13×10^{-4} | 2.73×10^{-2} 1.08×10^{-2} | 2.40×10^{10} | 28.13 |

*Pressure in mm corrected to 0°C.

†Distance between window and internal grid.

‡Depth of sensitive volume is 2.54 cm, except for experiment 13 which has a 6.65-cm depth.

#Attenuation factors for supporting meshes have been included in effective area calculations.

Table 2
Data Reduction Constants

| Experiment Number | Detector Conversion Constant, K (ergs/sec amp) | Wavelength Band (angstroms) | Assumed Graybody Temperature (10 ⁶ K) | Effective Area, A (cm ²) | Amplifier Range | Amplifier Slope, m (volts/amp) | Experiment Conversion Constant, C = K/Am (ergs/cm ² sec volt) | Amplifier Quiescent Level, b (volts) | Amplifier Calibration Level (volts) |
|-------------------|--|-----------------------------|--|--------------------------------------|-----------------|--------------------------------|--|--------------------------------------|-------------------------------------|
| 1 A | 7.229 × 10 ⁸ | 0.5 - 3 | 10 | 5.28 | 1 | 1.00 × 10 ¹³ | 1.37 × 10 ⁻⁵ | 0.34 | 3.60 |
| | | | | | 2 | 4.57 × 10 ¹¹ | 3.00 × 10 ⁻⁴ | 0.22 | 1.82 |
| | | | | | 3 | 2.03 × 10 ¹⁰ | 6.75 × 10 ⁻³ | 0.26 | 3.88 |
| | | | | | 4 | 9.23 × 10 ⁸ | 1.48 × 10 ⁻¹ | 0.20 | 3.12 |
| 1 B | 6.957 × 10 ⁸ | 0.5 - 3 | 10 | 16.17 | 1 | 1.04 × 10 ¹³ | 4.14 × 10 ⁻⁶ | 0.28 | 3.78 |
| | | | | | 2 | 4.70 × 10 ¹¹ | 9.15 × 10 ⁻⁵ | 0.30 | 1.94 |
| | | | | | 3 | 2.03 × 10 ¹⁰ | 2.12 × 10 ⁻³ | 0.32 | 4.02 |
| | | | | | 4 | 9.23 × 10 ⁸ | 4.66 × 10 ⁻² | 0.28 | 3.20 |
| 2 | 2.840 × 10 ⁹ | 1 - 5 | 2 | 5.28 | 1 | 4.80 × 10 ¹² | 1.12 × 10 ⁻⁴ | 0.30 | 4.28 |
| | | | | | 2 | 2.13 × 10 ¹¹ | 2.53 × 10 ⁻³ | 0.30 | 1.86 |
| | | | | | 3 | 1.01 × 10 ¹⁰ | 5.33 × 10 ⁻² | 0.30 | 4.88 |
| 3 A | 3.074 × 10 ⁹ | 1 - 8 | 2 | 2.97 | 1 | 4.83 × 10 ¹² | 2.14 × 10 ⁻⁴ | 0.36 | 4.21 |
| | | | | | 2 | 2.19 × 10 ¹¹ | 4.73 × 10 ⁻³ | 0.32 | 1.86 |
| | | | | | 3 | 1.01 × 10 ¹⁰ | 1.02 × 10 ⁻¹ | 0.34 | 4.68 |
| 3 B | 2.702 × 10 ⁹ | 1 - 8 | 2 | 2.97 | 1 | 9.93 × 10 ¹² | 9.16 × 10 ⁻⁵ | 0.28 | 3.64 |
| | | | | | 2 | 4.52 × 10 ¹¹ | 2.01 × 10 ⁻³ | 0.24 | 1.86 |
| | | | | | 3 | 2.02 × 10 ¹⁰ | 4.50 × 10 ⁻² | 0.24 | 3.88 |
| 4 A | 7.977 × 10 ⁹ | 8 - 20 | 2 | 1.12 | 1 | 7.11 × 10 ¹¹ | 1.00 × 10 ⁻² | 0.28 | 4.35 |
| | | | | | 2 | 3.21 × 10 ¹⁰ | 2.22 × 10 ⁻¹ | 0.27 | 2.89 |
| 4 B | 7.977 × 10 ⁹ | 8 - 20 | 2 | 0.40 | 1 | 4.85 × 10 ¹² | 4.11 × 10 ⁻³ | 0.36 | 3.50 |
| | | | | | 2 | 2.15 × 10 ¹¹ | 9.28 × 10 ⁻² | 0.32 | 1.86 |
| 5 | 2.434 × 10 ¹⁰ | 44 - 60 | 0.5 | 0.17 | 1 | 4.75 × 10 ¹¹ | 3.01 × 10 ⁻¹ | 0.28 | 4.16 |
| 6 | 6.116 × 10 ⁹ | 1 - 20 | 2 | 0.17 | 1 | 4.77 × 10 ¹¹ | 7.54 × 10 ⁻² | 0.22 | 4.12 |
| 7 A | 2.68 × 10 ⁸ | 1080 - 1350 | — | 2.68 × 10 ⁻³ | AC | — | — | 0.52 | 3.46 |
| | | | | | DC | 5.06 × 10 ¹⁰ | 1.98 × 10 ⁰ | 0.22 | 4.08 |
| 7 B | 1.96 × 10 ⁸ | 1080 - 1350 | — | 1.57 × 10 ⁻⁴ | 1 | 4.87 × 10 ¹¹ | 2.56 × 10 ⁰ | 0.26 | 4.20 |
| 8 | 3.85 × 10 ⁸ | 1225 - 1350 | — | 3.58 × 10 ⁻⁴ | 1 | 4.77 × 10 ¹² | 2.25 × 10 ⁻¹ | 0.32 | 4.28 |
| 9 | 8.06 × 10 ⁸ | 1450 - 1600 | — | 1.61 × 10 ⁻⁴ | 1 | 2.50 × 10 ¹² | 2.00 × 10 ⁰ | 0.30 | 4.38 |
| 10 A | 7.205 × 10 ⁸ | 0.5 - 3 | 10 | 5.28 | 1 | 2.39 × 10 ¹² | 5.71 × 10 ⁻⁵ | 0.36 | 4.28 |
| 10 B | 2.602 × 10 ⁹ | 1 - 8 | 2 | 2.97 | 1 | 4.76 × 10 ¹² | 1.84 × 10 ⁻⁴ | 0.30 | 4.16 |
| 11 | — | 0.08 - 0.8 | — | 10.0 | — | — | — | — | — |
| 12 A | 8.28 × 10 ¹⁰ | 170 - 500 | — | 1.93 | log | 1.274* | 10.6325* | 15.32* | 4.03 |
| | | | | | linear | 4.80 × 10 ¹⁰ | 8.94 × 10 ⁻¹ | 0.28 | 4.24 |
| 12 B | 1.21 × 10 ¹⁰ | 170 - 700 | — | 0.079 | log | 1.274* | 11.1847* | 15.32* | 4.03 |
| | | | | | linear | 4.80 × 10 ¹⁰ | 3.19 × 10 ⁰ | 0.28 | 4.24 |
| 13 | 2.768 × 10 ⁹ | 0.1 - 1.6 | 10 | 28.13 | 1 | 1.04 × 10 ¹³ | 9.46 × 10 ⁻⁶ | 0.40 | 4.59 |
| | | | | | 2 | 4.62 × 10 ¹¹ | 2.13 × 10 ⁻⁴ | 0.42 | 2.02 |
| | | | | | 3 | 2.03 × 10 ¹⁰ | 4.85 × 10 ⁻³ | 0.38 | 4.92 |
| | | | | | 4 | 9.17 × 10 ⁸ | 1.07 × 10 ⁻¹ | 0.38 | 3.28 |

*log₁₀ F = C + (V - b)/m.

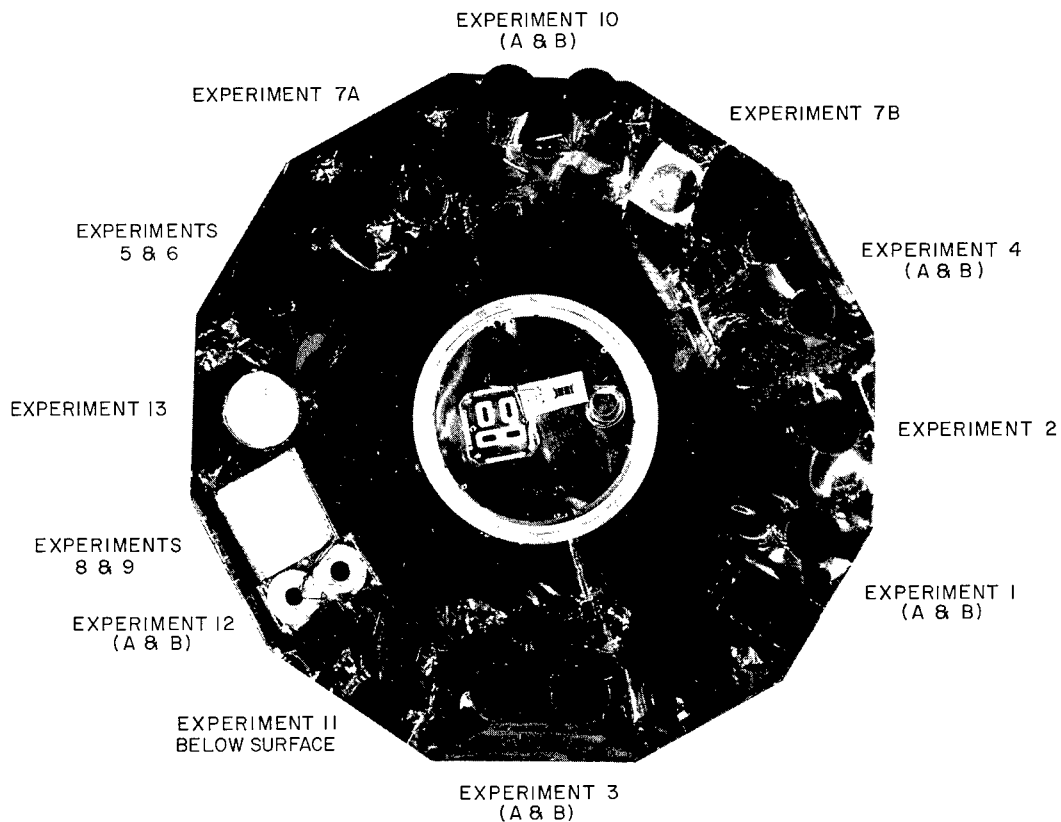


Fig. 2 — Location of the solar experiments and a direct view of the collimators. The experiment 12 sensors are missing in this photo. Note the four apertures for the fine-angle-aspect sensors in the center of the mounting flange. A multiple-layer Mylar-aluminum thermal blanket covers this solar-oriented surface.

The experiment is designed to continue monitoring the 0.5 to 3 Å band emission, which exhibits an extremely large flux increase during solar flares. Fluctuations in the 0.5 to 3 Å emission cause changes in the D layer of the ionosphere, which prevent the normal operation of some ionosphere-dependent systems. In addition, the data from experiment 1 can be used with the data from experiments 2 and 3 to calculate an electron temperature and make a size estimate for an emitting solar region.

Experiment 2: 1 to 5 Å Band

A single ionization chamber sensitive to the 1 to 5 Å band of the x-ray spectrum is designated experiment 2. The sensor is connected to a three-range electrometer-amplifier. There is no redundant detector or amplifier because this is a new experiment whose utility has not yet been verified by experience. Data from experiment 2 will be continuously transmitted in real time but will only be stored in the memory when chosen in preference to data from experiment 13 by ground command.

X rays in the 1 to 5 Å band are known to affect the D layer of the ionosphere and exhibit a large increase during solar flares. The data from experiment 2 will be used with the data from experiments 1 and 3 to calculate an electron temperature and make a size estimate for emitting solar regions. Experiment 2 is expected to be most useful for this purpose when the solar x-ray flux is so low that experiment 1 cannot produce data above the noise level of its amplifier.

Experiment 3: 1 to 8 Å Band

Two independent ionization chambers sensitive to the 1 to 8 Å band of the x-ray spectrum are designated 3A and 3B. The ionization chambers are identical to those flown on SOLRAD 9. For redundancy, each is connected to its own three-range electrometer-amplifier and fed from a different power converter. A ground command selects 3A or 3B data for transmission in real time and storage in the memory unit.

The experiment is designed to continue monitoring the 1 to 8 Å band, which exhibits a large flux increase during solar flares and affects the D layer of the ionosphere. The data from experiment 3 will also be used with those from experiments 1 and 2 to calculate electron temperatures and estimate sizes for emitting solar regions.

Experiment 4: 8 to 16 Å Band

Two identical, independent ionization chambers sensitive to the 8 to 16 Å band of the x-ray spectrum are designated 4A and 4B. The ionization chambers are identical to those used on SOLRAD 9. For redundancy, each is connected to its own two-range electrometer-amplifier and fed from a different power converter. A ground command determines whether 4A or 4B will be connected to the telemetry and data-storage systems. The experiment is designed to monitor the changes in x-ray flux which have proved to be useful indicators of a plage region's potential for solar flare activity. Although both of the 8 to 16 Å ionization chambers on SOLRAD 9 continue to function 48 months after launch, the experiment 4A detector on SOLRAD 10 failed within 2 months of launch.

The data conversion information for these detectors (p. 22) should be carefully noted. In converting the telemetered information to energy flux units, the most recent available mass absorption coefficients were used. These more recently measured coefficients are significantly different from the older values used when calculating conversion constants for 8 to 20 Å band flux from older NRL experiments and satellites. Therefore, to compare the 8 to 20 Å band flux obtained from experiment 4 of SOLRAD 10 with any earlier NRL 8 to 20 Å values, the SOLRAD 10 value for the 8 to 20 Å flux should be multiplied by 0.70.

Experiment 5: 1 to 20 Å, 44 to 60 Å Bands

Experiment 5 is a single ionization chamber sensitive to the 1 to 20 Å and 44 to 60 Å bands of the x-ray spectrum. The ionization chamber, which is identical to the one used on SOLRAD 9 to measure these bands, is connected to a single-range electrometer-amplifier. Data from experiment 6 will be used to remove the 1 to 20 Å contribution to

the experiment 5 detector response to allow continued monitoring of the 44 to 60 Å band, which shows a small flux increase during solar flares.

Experiment 6: 1 to 20 Å Band

Experiment 6 is a single ionization chamber sensitive to the 1 to 20 Å band of the x-ray spectrum. The ionization chamber, which is identical to the one used on SOLRAD 9 to monitor the 1 to 20 Å band, is connected to a single-range electrometer-amplifier. Data from the experiment will be used to remove the 1 to 20 Å contribution to the experiment 5 detector response.

Experiment 7A: Lyman-Alpha Flare Detector

Experiment 7A uses a lithium fluoride lens to focus an image of the solar disk in the Lyman-alpha line of hydrogen (1216 Å) on a matrix of pinholes shielding an ionization chamber sensitive to the 1080 to 1350 Å band of the ultraviolet spectrum. It is designed to detect localized enhancement of Lyman-alpha radiation accompanying solar flares. By maintaining the spin axis of the satellite to within 3° of the satellite-sun line, the solar image will always fall somewhere on the matrix of pinholes. The satellite's spin motion moves this solar image on the matrix and causes the pinholes to chop the light output coming from small areas of enhanced brightness on the solar disk. Each pinhole has an area approximately 10^{-3} that of the projected solar image. The current generated in the detector during a solar flare is expected to resemble a dc bias level with an ac ripple superimposed on it. The dc bias level is a measure of the total ultraviolet flux from the sun in the 1080 to 1350 Å band which is dominated by the 1216 Å line emission. The ac ripple is a quantitative measure of the nonuniformity of the sun's 1216 Å emission on a scale up to 10^{-3} of the area of the solar disk. This scale size is expected to provide a sensitive indicator of flare activity. Unfortunately, the experiment failed within a month of launch without observing a solar flare capable of stimulating an ac response in the amplifier.

Experiment 7B: 1080 to 1350 Å Band

Experiment 7B is a pair of ionization chambers sensitive to the 1080 to 1350 Å band of the ultraviolet spectrum and connected in parallel to a single-range electrometer-amplifier. Solar emission in the 1080 to 1350 Å band is strongly dominated by the Lyman-alpha line of hydrogen (1216 Å). Therefore, this experiment will really be monitoring the sun's Lyman-alpha emission. A truer measure of the Lyman-alpha variations can be obtained by using the data from experiment 8 to remove any contribution from variations in the ultraviolet continuum near the Lyman-alpha line.

Experiment 8: 1225 to 1350 Å Band

Experiment 8 is a pair of ionization chambers sensitive to the 1225 to 1350 Å band of the ultraviolet spectrum and connected in parallel to a single-range electrometer-amplifier. This experiment will monitor the behavior of the ultraviolet continuum in the vicinity of the Lyman-alpha line of hydrogen at 1216 Å. Emission data from this experiment can be used to correct the data from experiment 7B to isolate the Lyman-alpha line emission.

Experiment 9: 1450 to 1600 Å Band

Experiment 9 is a pair of ionization chambers sensitive to the 1450 to 1600 Å band of the ultraviolet spectrum and connected in parallel to a single-range electrometer-amplifier. This experiment will monitor the behavior of the ultraviolet continuum.

Experiment 10: Charged Particle Indicators

Two independent ionization chambers, each connected to a single-range electrometer-amplifier and fed from a different power converter, are designated 10A and 10B. Experiment 10A uses a sensor identical to that of experiment 1A; experiment 10B uses a sensor identical to those of experiment 3. Both sensors are mounted on the satellite surface which faces the sun but are aligned at a 15° angle to the spin axis. A 5° half-angle collimator for each sensor prevents them from observing the sun when the attitude control system is operating properly. Therefore, current generated in these sensors will be of nonsolar origin and almost certainly due to charged particles trapped in the Earth's magnetic field which can affect the solar x-ray experiments. These charged particles are able to penetrate a detector's window or walls and, in the case of the solar x-ray detectors, generate current which cannot be distinguished from current generated by solar emission. Data from both 10A and 10B will be continuously transmitted in real time, but a ground command will select data from only one for storage in the memory unit.

Experiment 11: 15 to 150 keV

Experiment 11 is a CsI(Na) scintillating crystal surrounded by a plastic scintillating material viewed by a single photomultiplier. This experiment is designed to collect data on the very-high-energy solar x-ray emission which is present only during solar flares. The electrical pulses generated in the photomultiplier are amplified, and pulses equivalent to solar x-ray energies between 15 and 150 keV (0.8 to 0.08 Å) are sorted into four energy ranges: 15 to 20, 20 to 30, 30 to 60, and 60 to 150 keV. The number of pulses observed in a 6.36-second interval in each range is transmitted in real time every 6.4 seconds. The total number of pulses observed in a 48.8-second interval over the entire 15- to 150-keV range is stored in the satellite's memory unit. An americium 241 radioactive source can be moved into the detector's field of view for in-flight calibration of the experiment.

High-energy charged particles can cause visible light emission in the scintillating crystal and in the plastic material. Electronic rise-time discrimination is used to separate the fast, particle-induced pulses in the plastic from the slower pulses produced in the CsI by x rays and particles. Only pulses caused by x rays are subjected to pulse-height analysis or stored in the memory. A ratemeter monitors the number of particle-induced pulses as a measure of the false counts created in the CsI by cosmic rays or charged particles trapped in the Earth's magnetic field. The ratemeter data are transmitted in real time only.

Experiment 12: 170 to 700 Å Band

Experiment 12 is a pair of detectors, each having a LiF photosensitive surface behind a pair of aluminum filters, whose output is fed into either a linear or a logarithmic electrometer-amplifier. The detector designated 12A has a pair of carbon filters in addition

to the two aluminum filters, which greatly reduce its sensitivity in the 500 to 700 Å range. Unfortunately, this detector has produced abnormally low readings since launch. A ground command selects the amplifier whose data are to be presented to the real-time telemetry and memory systems. Either detector can be connected by ground command to the selected amplifier. Since the 12B detector is the only one of the pair which is operating properly and it produces current within the range of operation of the linear electrometer-amplifier, the 12B detector with the linear amplifier will be the normally selected combination. The experiment is designed to provide information about the extreme ultraviolet spectrum, which causes ionospheric F-layer excitation.

Experiment 13: 0.1 to 1.6 Å Band

Experiment 13 is a single-ionization chamber with a large window area connected to a four-range electrometer-amplifier. The experiment will monitor the hard x-ray emission in the 0.1 to 1.6 Å band, which is observed only during solar flares. Data from this experiment will be compared with data from experiment 11, which is also observing hard x-ray emission from solar flares. Data from experiment 13 will be continuously transmitted in real time but will only be stored in the memory unit when chosen in preference to data from experiment 2 by ground command.

Experiment 14: Satellite Temperature Monitor

Experiment 14 is a standard resistance thermometer located on the antisun surface of the satellite and thermally isolated from the satellite structure. The purpose of the experiment is to measure the lowest temperature attained by the sensor and the variability of this temperature with time. The sensor is mounted on a 30-layer thermal isolation blanket attached to the second of a set of two fiberglass radiators which are connected by materials of low thermal conductivity. Radiative isolation between the fiberglass radiators is enhanced by using gold tapes and thermal control coatings. Data from this experiment are transmitted in real time only. Information received will be useful when designing future experiments which require low temperatures for successful operation.

Stellar X-Ray (Stellrad) Experiment

The Stellrad experiment uses a proportional counter sensitive to 0.5 to 15 Å x rays and seven-channel pulse-height analysis to locate and provide spectral information about nonsolar x-ray sources. The detector is mounted on the side of the spacecraft and aligned perpendicular to the spin axis. The detector's window is made of 1/8 mil Mylar with an effective area of 100 cm². The gas filling is a mixture composed of 0.45 argon, 0.45 xenon, and 0.10 carbon dioxide maintained at 4-lb/in² pressure by regulation-controlled replenishment from a reservoir. A collimator limits the field of view to 8° (full-width at half-maximum) in a plane containing the spin axis and 1° (fwhm) in the plane perpendicular to the spin axis. Charged-particle interference information is provided by proportional counters mounted on three sides of the x-ray detector.

Aspect information is provided by a blue-sensitive photomultiplier capable of detecting all fourth-magnitude and hot fifth-magnitude stars. Two aspect sensors are provided for

redundancy. The resolution of the aspect system and the accuracy with which the experiment can locate x-ray sources is better than $\pm 0.25^\circ$. This resolution is limited by the satellite spin rate and the telemetry, rather than by the sensors.

Protection From Trapped Charged Particles

Concentrations of trapped charged particles capable of penetrating the windows or walls of the sensors are encountered in the polar regions on every orbit and whenever the orbital path passes through the South Atlantic Magnetic Anomaly. After entering the ionization chamber, these particles create ionization which is indistinguishable from that produced by solar radiation. If the electrometer-amplifier used with the ionization chamber is relatively insensitive, such as those used with experiments measuring radiation whose wavelength is greater than 20 Å, the currents generated by the penetrating charged particles will rarely be above the noise level of the electronics. However, the current generated in the more sensitive electrometer-amplifiers used with those experiments measuring radiation with wavelengths shorter than 20 Å will frequently be many times greater than the current normally produced by solar radiation. The problem of charged-particle interference does not usually affect satellites in low-inclination orbits. However, a low-inclination orbit was not selected for SOLRAD 10 because of the location of the NRL ground station at Blossom Point, Maryland. In addition, a low-inclination orbit would eliminate the participation of COSPAR stations located at higher latitudes.

Although it is recognized that the interference by trapped charged particles cannot be completely eliminated while constrained to a higher-inclination orbit, steps to decrease the severity of the effects were taken. The apogee was planned to be less than 400 naut mi to stay below the regions of higher trapped-particle concentration. Experiments 3A, 3B, 4A, 4B, 5, 6, and 10B are equipped with magnets to deflect some of the approaching charged particles away from the detectors' windows. The magnets used for experiments 5 and 6 are 0.5 inch thick, with a 0.35-inch gap and a magnetic induction of 3000 gauss; the inner surface of each magnet is located 0.25 inch away from the detector's window aperture. The magnets used for the other experiments mentioned above are 1.0 inch thick with a 0.725-inch gap and a magnetic induction of 2000 gauss; each is mounted with the inner surface touching the window aperture. The pole faces of all magnets are covered with a layer of beryllium to reduce x-ray generation at the pole faces by bremsstrahlung. Experiments 1A, 1B, 2, 3A, 3B, 4A, 4B, 5, 6, 10A, and 10B are equipped with aluminum collimators to diminish the solid angle through which charged particles can approach a detector's window unimpeded. All collimators are designed so that a point source located within a cone of 5° half-angle will be able to illuminate every portion of the detector's aperture. The walls of the collimators used for experiments 1A, 1B, and 2 are 0.094 inch thick. The other collimators have walls 0.031 inch thick. For protection from particles, experiment 11 is completely enclosed within the skin of SOLRAD 10. The x rays measured are of sufficiently high energy that they can penetrate the satellite's skin and reach the scintillating crystal. High-energy particles can also penetrate to the sensor; therefore, experiment 11 also uses rise-time analysis to distinguish light pulses in the plastic material due to charged particles from light pulses in the CsI crystal due to x rays and charged particles.

As a positive indicator of interference by trapped charged particles, the sensors for experiment 10 are aligned at a 15° angle to the satellite's spin axis and prevented from observing the sun by the 5° half-angle aluminum collimators. Therefore, current generated

in the sensors cannot be due to solar electromagnetic radiation and will almost certainly be due to trapped charged particles. If no current is being generated in the experiment 10 sensors, data from the solar experiments are almost certainly free of particle interference.

EXPERIMENT ELECTRONICS

The range-changing and calibration sequences for the experiment electrometer-amplifiers are described in detail in this section. Some information about the telemetry and data-storage systems is also given, but primarily in connection with their interactions with the range-changing and calibration sequences. Detailed information about the telemetry and memory systems will be found in subsequent sections of this report.

Electrometer-Amplifier Range Changes

The enhancement in solar x-ray emission observed during solar flares varies from three or four orders of magnitude above preflare levels for the 0.5 to 3 Å band to less than one order of magnitude for the 44 to 60 Å band. When the enhancement is greater than an order of magnitude, it is impossible to make satisfactory measurements over the entire emission range using a single-range linear electrometer-amplifier. Therefore, experiments designed to monitor x-ray emission in the shorter wavelength bands use single-range logarithmic electrometer-amplifiers or multirange linear electrometer-amplifiers. The shorter-wavelength experiments on SOLRAD 10 are all equipped with multirange electrometer-amplifiers, and Table 3 identifies all multirange experiments and the number of ranges available to each of them.

Table 3
SOLRAD 10 Multirange Experiments

| Experiment | Number of Ranges |
|------------|------------------|
| 1 | 4 |
| 2 | 3 |
| 3 | 3 |
| 4 | 2 |
| 13 | 4 |

Each range of a multirange experiment is identified by number, e.g., range 1 or range 3. Range 1 is the most sensitive mode of operation for an experiment. Therefore, a well-designed solar x-ray experiment will operate in range 1 when solar activity is at a low level. As the identifying number for a range increases, the sensitivity of the experiment decreases. Therefore, range 2, 3, or 4 operation would be expected only during periods of enhanced solar activity. For this report, the process of shifting from a more sensitive to a less sensitive range, e.g., from range 2 to range 3, will be called "downranging," and shifting from a less to a more sensitive range will be called "upranging."

Automatic Range Changing

A single command from the ground station will put all multirange experiments into their most sensitive range, range 1, and enable them to change ranges automatically. Subsequently, an automatic range change occurs whenever the voltage output of an electrometer-amplifier falls outside of a range of voltage levels bounded by a pair of preset voltages in the range change circuitry. If an electrometer-amplifier's output exceeds 4.8 volts and it is not already in its least sensitive range, it is forced to downrange. If an electrometer-amplifier's output is less than 0.6 volt and it is not already in its most sensitive range, it is forced to uprange. Overlapping coverage in the ranges is provided by making the current equivalent to a 4.8-volt output on the more sensitive range equal to the current which is equivalent to an output of 0.5 volt on the less sensitive range. Since most of the amplifiers have a quiescent (no input) level at approximately 0.3 volt, a 0.5-volt signal observed on a less sensitive range after a range change will be measurably above the quiescent level.

The sequence of events which make up one complete automatic range change cycle is controlled by two pulses. The primary pulse occurs at 1-minute intervals and defines the basic period of one complete range change cycle. The secondary pulse occurs at 4-second intervals and triggers each of the events which make up the automatic range change sequence. For redundancy, each of these pulses can be generated from two independent sources. Figure 3 shows the sequence of events for automatic range changing and memory sampling.

The primary pulse enables the automatic range change electronics to accept the secondary pulses and carry out an automatic range change sequence. Since the primary and secondary pulses are not synchronized, the first secondary pulse which can be accepted can occur anytime within 4 seconds after the primary pulse occurs. The first acceptable secondary pulse will cause a multirange electrometer-amplifier whose output is less than 0.6 volt to uprange, assuming that it is not already in range 1. The next four secondary pulses, which occur at 4-second intervals, will each cause a multirange electrometer-amplifier whose output is greater than 4.8 volts to downrange, assuming that it is not already in its least sensitive range. Therefore, within 20 seconds after the primary pulse occurs, there will be one opportunity for an electrometer-amplifier to uprange, and four opportunities for it to downrange. For the next 16 seconds no automatic range changing can occur because the sixth through eighth secondary pulses of each automatic range change cycle do not trigger any events. The ninth secondary pulse will provide another opportunity to uprange, and the tenth through thirteenth pulses will each provide an opportunity to downrange. No more secondary pulses will be accepted after the thirteenth until a new automatic range change cycle is begun by the next primary pulse. Therefore, multirange electrometer-amplifiers can uprange once and downrange up to four times every 30 seconds.

The thirteenth secondary pulse of the automatic range change cycle also initiates the scan of the output of all of the electrometer-amplifiers to obtain the data sample which will be stored in the memory just prior to the occurrence of the next primary pulse. The scan of the electrometer-amplifiers takes about 3 seconds, and the scanning sequence is arranged so that the multirange electrometer-amplifiers are scanned last to give them time to stabilize after a range change.

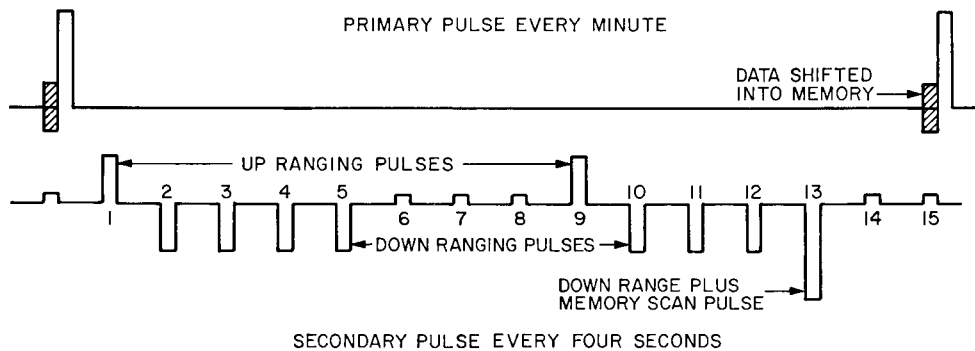


Fig. 3 — Timing diagram for automatic range change sequence and shifting data sample into memory. Although secondary pulses are shown with different shapes for different functions, all secondary pulses are electronically identical. The primary and secondary pulse trains are not synchronized. Therefore, the first secondary pulse can occur any time within 4 seconds after a primary pulse.

Manual Range Changing

When the experiments are operating in an automatic range changing mode, an individual command must be sent to each multirange experiment which is to be shifted to the manual range changing mode. The manual mode command shifts the experiment's electrometer-amplifier to its most sensitive range, range 1, and prevents it from responding to the automatic range changing pulses. Once the selected experiments have been individually commanded to the manual range changing mode, a common, ground-generated, manual ranging pulse will cause all of them to shift to the next less sensitive range each time the manual ranging pulse is sent until the least sensitive range is reached. The manual ranging pulses can only shift experiments to less sensitive ranges. When a given experiment has been manually commanded to the desired range, a disable command addressed to that experiment alone will allow it to ignore subsequent manual ranging pulses. Once the disable command is sent to an experiment, subsequent range changing for that experiment can occur only if the automatic mode command is sent or if the manual mode command for that experiment is sent again. Resending the manual mode command will affect only the selected experiment by shifting it to range 1 and allowing it to respond to manual ranging pulses again. Sending the automatic mode command will affect *all* multirange experiments by shifting them to range 1 and allowing them to respond to the automatic range changing pulses again. When an experiment is operating in the manual mode, its data are still sampled for memory storage during the normal scan sequence controlled by the automatic range changing pulses.

Electrometer-Amplifier Calibration Sequence

The sequence to calibrate the electrometer-amplifiers of all experiments except experiments 11, 14, and Stellrad can be initiated either by a specific command for this purpose or by the command to transmit the data stored in the memory unit if the memory is not sampling in the "flare mode." The sequence starts by disconnecting each detector from its electrometer-amplifier and connecting calibration resistors for each experiment and range which will cause a characteristic voltage output if the electrometer-amplifier is

working correctly. Multirange electrometer-amplifiers operating in the automatic range change mode will then be carried through a cycle in which they start in range 1 and are forced to downrange every 4 seconds until their least sensitive ranges are reached. They remain in their least sensitive ranges until 32 seconds have passed since the calibration sequence began. Then they will all revert to range 1 and step through the ranges at 4-second intervals until their least sensitive ranges are reached again. They remain in their least sensitive ranges for the remainder of the 57-second calibration sequence.

The data sample which will be stored in the memory is obtained during these final few seconds of the calibration cycle while the amplifiers are held in their least sensitive ranges. Multirange electrometer-amplifiers operating in the manual range change mode remain fixed throughout the calibration cycle in whatever range they were in prior to the beginning of the cycle. The calibration sequence ends with the multirange electrometer-amplifiers operating in the automatic range change mode left in their least sensitive ranges. Since only one upranging shift can occur automatically each 30 seconds, normally 60 to 90 seconds must pass after the calibration sequence ends before the four-range electrometer-amplifiers begin producing data above the quiescent level if range 1 is the proper operating range.

Although calibration data for only one range of a multirange electrometer-amplifier are stored in the memory for each calibration sequence, the data for all ranges are transmitted in real time. In addition, calibration data for any one range of a multirange electrometer-amplifier can be stored in the memory by using the manual range change mode to shift to the selected range and leaving the electrometer-amplifier in the manual range change mode at the selected range throughout the calibration cycle.

It should be noted that these calibration data pertain only to the electrometer-amplifiers and their associated electronics. Except for experiment 11 there is no way to calibrate the detectors.

DATA TRANSMISSION

Telemetry Systems

There are two telemetry systems aboard SOLRAD 10 to transmit four main data forms: stored data, real-time digital (PCM) data, real-time analog data, and Stellrad data. Telemetry system 1 (TM 1) uses a pulse-amplitude-modulated, pulse-code-modulated, frequency-modulated, phase-modulated (PAM-PCM-FM-PM) transmitter which operates at 137.710 MHz with a radiated power of 250 milliwatts. Normally, TM 1 continuously transmits analog and PCM real-time data. The outputs from five frequency-modulated IRIG voltage-controlled subcarrier oscillators (VCO) are linearly mixed and phase modulate the rf carrier. Telemetry system 2 (TM 2) uses a PCM-PM transmitter which operates at 136.380 MHz with a radiated power of 250 milliwatts. A power amplifier can be commanded into TM 2 to raise the radiated power to 5 watts. TM 2 transmits stored data or Stellrad data on command. For redundancy, TM 2 can be used to transmit the real-time PCM data and TM 1 can be used to transmit stored data or Stellrad data. Since the real-time analog and PCM data forms carry the same information, it is not necessary to have the capability to transmit both forms on TM 2. However, since TM 2 is not designed to transmit continuously and is equipped with a 15-minute timer to prevent continuous

transmission, a failure in TM 1 would prevent recording of real-time data except over a ground station capable of commanding TM 2 into operation.

Primary Real-Time Data Transmission — PCM

Although SOLRAD 10 transmits data continuously in real time in both digital and analog formats on TM 1, the primary real-time transmission format is digital (PCM). Data from all experiments except Stellrad are included in the real-time PCM data. The PCM real-time telemetry system has an encoder which converts analog signals from the experiments and housekeeping information into digital format and controls the sequence in which the digital data are passed along the telemetry system. Digital data from experiment 11, various digital housekeeping data, and digital status information for the electrometer-amplifier range and A or B detector identification are put in proper sequence by the encoder. Although only one encoder is needed, two are present for redundancy.

The main frame of the PCM real-time telemetry system contains ten eight-bit words. Two of the ten words are used for synchronization, and the remainder are used for subcommutated experiment and housekeeping data. Ten complete main frame cycles, a total time of 1.6 seconds, are required to complete one subcommutator cycle. Experiments 2, 4, 5, 6, 8, 9, 10A, 10B, 12, 13, and 14 each have one subcommutator word and their sampling interval is therefore 1.6 seconds. Experiments 1 and 3 each have two evenly spaced subcommutator words to give them an 0.8-second sampling interval. Experiment 7A has a separate subcommutator word for its ac and dc components and maintains a 1.6-second sampling resolution for each. Experiment 11 has three eight-bit subcommutator words. It uses 14 bits to display the number of counts in one of its four channels on each subcommutator cycle. Two bits are used to identify the channel. It takes four subcommutator cycles, 6.4 seconds, to transmit a complete set of information from this four-channel experiment. The third word provides data from the ratemeter on experiment 11, which monitors the number of pulses produced in the plastic shield by charged particles.

The conversion of analog voltages from the electrometer-amplifiers to digital values by the encoder uses 256 levels to cover the range from 0.0 to 5.1 volts. Therefore, the voltage resolution for the normal analog-to-digital conversion is 20 millivolts. To provide greater resolution for experiment 7B, the three most significant bits from the normal conversion process are used to set one of eight voltage levels with a 0.6375-volt separation between 0.0000 and 4.4625 volts. The difference between the voltage from the electrometer-amplifier for experiment 7B and the set voltage level is increased by a factor of eight, and this expanded voltage difference is then converted to a digital value by the normal process. Therefore, 256 levels are used to cover the range from 0.0000 to 0.6375 volt, which provides a resolution of 2.5 millivolts.

The digital value obtained from the normal analog-to-digital conversion of the experiment 7B data is given by one subcommutator word. Another adjacent subcommutator word gives the value of the expanded difference between the electrometer-amplifier's voltage and the voltage level based on the three most significant bits produced by the normal conversion process. Therefore, the voltage from the electrometer-amplifier for experiment 7B can be obtained with a resolution of 2.5 millivolts from

$$V = 0.6375A + 0.0025B, \quad (1)$$

where A is the value of the three most significant bits from the normal conversion and B is the value of the eight bits of the word giving the expanded voltage difference.

A time reference is provided in the stream of data. The PCM encoder has a crystal oscillator which causes an eight-bit time vernier counter to increment every 0.8 second. The contents of this time vernier are displayed in a subcommutator word which is transmitted every 1.6 seconds. The eight-bit vernier counter overflows at intervals of 3.4133 minutes, and the overflow increments a 16-bit absolute time counter. Each time the absolute time counter increments, its value is displayed in two subcommutator words which are shared with housekeeping information.

The real-time PCM data are normally transmitted continuously by the TM 1 transmitter along with the analog real-time data and various satellite housekeeping information. The PCM data modulate the voltage-controlled subcarrier oscillator for IRIG channel 12 and are actually transmitted in an analog transmission mode. It is also possible to have the PCM real-time data bypass the IRIG 12 subcarrier oscillator and feed directly into the TM 1 transmitter. In this case there would be no analog format transmission, and continuous transmission of all information, except the PCM real-time data, would cease. Since the PCM and analog real-time data are redundant in experiment data and essential housekeeping information, the loss of transmission capability for analog format data would not seriously affect the overall performance of the satellite. If the transmitter of TM 1 ceased to function, the PCM real-time data could be transmitted by the TM 2 transmitter. Since the TM 2 transmitter is equipped with a 15-minute timer to prevent continuous transmission, a failure of the TM 1 transmitter would prevent transmission of real-time data except over a ground station capable of commanding the TM 2 transmitter into operation.

Secondary Real-Time Data Transmission — Analog

The secondary real-time transmission format will be analog, and all experiments except experiment 11 and Stellrad will appear in this format. Data to be transmitted in the analog format modulate the voltage-controlled subcarrier oscillators for IRIG channels 5 through 8. Since the real-time analog data are considered to be backup for the real-time PCM data, there is no redundancy in the subcarrier oscillator. Analog format transmission can be done only by the TM 1 transmitter, and so a failure of the TM 1 transmitter would prevent transmission of analog format data.

Data, status, and housekeeping information on IRIG channels 5 through 7 normally appear on 32-segment commutators which are transmitted at a rate of 8 segments per second. The channel 5 commutator contains one segment each for experiment 14 and the ac and dc components of experiment 7A. The remainder of the segments are devoted to housekeeping information for the satellite. The channel 6 commutator is completely devoted to housekeeping information and contains no experiment data. The channel 7 commutator contains data, range information, and detector identification for experiments 1 through 6, 7B, 8, 9, 10A, 10B, 12, and 13, and information indicating the angle between the satellite's spin axis and the satellite-sun line (aspect angle). This arrangement was made so that interested observers can obtain all the information needed to interpret the solar experiments' data by monitoring a single IRIG channel.

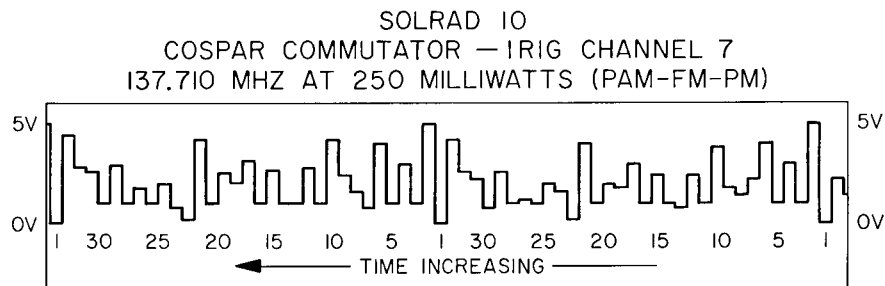


Fig. 4 — A sample record from the telemetry of SOLRAD 10 on IRIG channel 7. This channel carries data and status information for almost every solar experiment on a 32-segment commutator. The zero-volt calibrate of segment 1 followed by the 5-volt calibrate of segment 2 is a unique combination which can be used as a reference point in identifying the segments.

Channel 7 of SOLRAD 10 is commonly referred to as the “COSPAR Channel.” A sample of the channel 7 telemetry is shown in Fig. 4. Table 4 gives the COSPAR channel segment assignments and the meaning of the voltage levels for the range information and detector identification segments. All range information, detector identification, and aspect angle* information is given once every 4 seconds. Data from experiments 5, 6, 7B, 8, 9, 10A, 10B, and 12 also appear with a 4-second sampling interval. Data from experiments 2, 4, and 13 have a 2-second sampling interval, and data from experiments 1 and 3 have a 1.33-second sampling interval.

No experiment data appear on channel 8. Satellite status and housekeeping information on channel 8 do not appear on a commutator. As an optional mode of operation, it is also possible to present some status information on channels 5 and 6 without using a commutator. However, the COSPAR channel, channel 7, does not have any optional modes of operation. It will always present the same information using a 32-segment commutator.

Stored Data Transmission — Memory Data

The 54-kilobit capacity core memory on SOLRAD 10 is identical to the memory still operating on SOLRAD 9 after 48 months. It is programmed to store one data sample each minute for up to 14.25 hours. It accepts 48 digital bits of information as a standard data sample and is indifferent to the allocation of the 48 bits among the various experiments. This feature made possible a multiplexing operation external to the memory which allowed some choice in selecting experiments to be stored. Therefore, the experiments selected for storage in the memory are divided into one primary (P) and three secondary (S1, S2, and S3) groups. The primary group uses 31 bits and each secondary group uses 17 bits. Each standard data sample contains the primary group of experiments and one of the secondary groups.

The multiplexer has two modes of operation — a normal mode and a flare mode. When normal mode operation is selected, primary group data are stored every minute and

*The aspect angle indicator on IRIG channel 7 is not working properly. There is now no way to obtain aspect information from the analog telemetry. The aspect angle can be determined from the PCM telemetry only. Current aspect angle information will appear in the Spacewarn Bulletin.

Table 4
 COSPAR Channel -- IRIG Channel 7 Segment Assignments

| Segment | Function | Description |
|---------|--|---|
| 1 | Calibration | 0.0 Volt |
| 2 | Calibration | 5.0 Volt |
| 3 | Experiment 1 -- Detector Identification | 1.0 Volt -- 1B Detector; 3.0 Volt -- 1A Detector |
| 4 | Experiment 3 -- Detector Identification | 1.0 Volt -- 3B Detector; 3.0 Volt -- 3B Detector |
| 5 | Experiment 4 -- Detector Identification | 1.0 Volt -- 4B Detector; 3.0 Volt -- 4B Detector |
| 6 | Experiment 12 -- Detector and Amplifier Identification | 1.0 Volt -- 12B Detector, Log Amp; 2.0 Volt -- 12B Detector, Lin Amp; 3.0 Volt -- 12A Detector, Log Amp; 4.0 Volt -- 12A Detector, Lin Amp |
| 7 | Experiment 10A -- Data | -- |
| 8 | Experiment 12 -- Data | -- |
| 9 | Experiment 1 -- Data | -- |
| 10 | Experiment 3 -- Data | -- |
| 11 | Experiment 3 -- Range | 1.0 Volt -- Range 1; 2.0 Volt -- Range 2; 3.3 Volt -- Range 3 |
| 12 | Experiment 4 -- Data | -- |
| 13 | Experiment 13 -- Data | -- |
| 14 | Experiment 13 -- Range | 1.0 Volt -- Range 1; 2.0 Volt -- Range 2; 3.3 Volt -- Range 3; 4.7 Volt -- Range 4 |
| 15 | Experiment 2 -- Data | -- |
| 16 | Experiment 2 -- Range | 1.0 Volt -- Range 1; 2.0 Volt -- Range 2; 3.3 Volt -- Range 3 |
| 17 | Experiment 5 -- Data | -- |
| 18 | Experiment 6 -- Data | -- |
| 19 | Experiment 1 -- Data | -- |
| 20 | Experiment 1 -- Range | 1.0 Volt -- Range 1; 2.0 Volt -- Range 2; 3.3 Volt -- Range 3; 4.8 Volt -- Range 4 |
| 21 | Experiment 3 -- Data | -- |
| 22 | Solar Aspect | Not working properly.* |
| 23 | Experiment 10B -- Data | -- |
| 24 | Experiment 7B -- Data | -- |
| 25 | Experiment 8 -- Data | -- |
| 26 | Experiment 9 -- Data | -- |
| 27 | Experiment 4 -- Range | 1.0 Volt -- Range 1; 2.0 Volt -- Range 2 |
| 28 | Experiment 4 -- Data | -- |
| 29 | Experiment 13 -- Data | -- |
| 30 | Experiment 1 -- Data | -- |
| 31 | Experiment 2 -- Data | -- |
| 32 | Experiment 3 -- Data | -- |

*If working properly, positive voltage less than 0.5 volt would indicate that the aspect angle is less than 4 degrees.

the data from the three secondary groups are sequenced over three memory samples. Therefore, in normal mode operation data for the primary group have a 1-minute sampling interval and the data from each secondary group have a 3-minute sampling interval. When flare mode operation is selected, data from the primary group and the S1 secondary group are stored every minute. Data for the S2 and S3 secondary groups are never stored during flare mode operation. Shifting from one mode of operation to the other can be done automatically or by ground command. The automatic mode changes are triggered by the shift between range 1 and range 2 of the experiment 3 electrometer-amplifier which is connected to the real-time telemetry. The memory sampling mode automatically changes to flare mode when the electrometer-amplifier shifts to range 2 and reverts to normal sampling mode when the electrometer-amplifier returns to range 1. The transition between ranges 1 and 2 is equivalent to a solar energy flux of 9.5×10^{-4} ergs/cm²sec for experiment 3A and 4.1×10^{-4} ergs/cm²sec for experiment 3B. It is also possible to lock the multiplexer into either mode by ground command so that automatic sampling mode changes cannot occur.

The composition of the primary and secondary experiment groups and the bit allocations are given in Table 5. A five-bit analog-to-digital conversion is used to encode the voltage from the experiment electrometer-amplifiers. Therefore, the voltage resolution for the data stored in the memory is 0.160 volt. In the case of experiment 10, only the four least significant bits of the five-bit conversion are stored in the memory. If the analog-to-digital conversion for experiment 10 requires more than 15 digital counts, the four least significant bits stored in the memory will be locked at the value of 15. Digital data from all four channels of experiment 11 are accumulated for a 48.8-second period, compressed, and stored in the nine bits allocated in secondary group S1. In Table 5, the column titled "Range Bits" gives the number of bits allocated to provide electrometer-amplifier range information for the primary group experiments and to provide identification of experiment 7A data as the ac or dc component. The dc component of the experiment 7A data appears every fifth time the S1 secondary group's data appear.

In the case of experiments 1, 3, 4, and 12, whichever detector is connected to the real-time telemetry system will have its data presented to the memory system. The selection of the A or B detector for those experiments for presentation to the memory and real-time transmission is by ground command. Although both 10A and 10B have their data telemetered in real time, only one of them can be connected to the memory system. The selection of 10A or 10B data for presentation to the memory is controlled by ground command. A ground command also chooses the data for either experiment 2 or 13 for storage in the memory system. Data from the experiment which is not connected to the memory system are transmitted in real time only. Data from experiment 14 and Stellrad are never stored in the memory.

In addition to the 15 bits accounted for in Table 5 for each secondary group, two additional bits are used to identify the secondary group whose data are contained in a standard sample. These two additional bits also indicate whether experiment 2 or experiment 13 data are included in the primary group.

In addition to the 48 digital bits allocated for the standard data sample, 16 bits are allocated in the memory to give a time reference for each standard data sample. The satellite contains a timing mechanism which increments a 16-bit absolute time counter at exactly 4-minute intervals. For reference with ground time, the value in the absolute

Table 5
Memory Allocation

| Experiment | Group | Data Bits | Range Bits |
|------------|-------|-----------|------------|
| 1A or 1B | P | 5 | 2 |
| 3A or 3B | P | 5 | 2 |
| 4A or 4B | P | 5 | 1 |
| 10A or 10B | P | 4 | 0 |
| 2 or 13 | P | 5 | 2 |
| 7A | S1 | 5 | 1 |
| 11 | S1 | 9 | 0 |
| 7B | S2 | 5 | 0 |
| 8 | S2 | 5 | 0 |
| 9 | S2 | 5 | 0 |
| 5 | S3 | 5 | 0 |
| 6 | S3 | 5 | 0 |
| 12A or 12B | S3 | 5 | 0 |

time counter appears in the analog real-time telemetry on IRIG channel 8 as it is incremented. After the data contained in the memory are read out and transmitted, which takes slightly more than 8 minutes, the memory waits for the timing mechanism to increment the absolute time counter before starting to store data again. The first frame of data stored in the memory contains the newly incremented value for the absolute time counter in the 16 bits allocated for time reference. Subsequent memory frames are numbered sequentially from 2 to 855 in the time reference bits. This provides a time reference for each data sample relative to the absolute time reference contained in the first frame. Since the memory stores a frame of data at exactly 1-minute intervals, the time at which a given data sample was stored can be established.

If the memory is sampling in the normal mode when the readout of the stored data commences, the command to read out the stored data will also initiate the calibration of the experiment electrometer-amplifiers. In this case the calibration sequence will be completed before the memory begins to store data again after the memory readout. However, calibration data as described in the section titled "Electrometer-Amplifier Calibration Sequence" are held in storage registers until the memory unit is ready to store data again; then the calibration data are stored in the first frame of memory. However, storage of calibration data is not limited to the first frame of the memory. If the specific command to calibrate the electrometer-amplifiers is sent while the memory is sampling, the storage of the calibration data is controlled by the normal scan sequence initiated by the automatic range changing pulses. If the memory is sampling in the flare mode when the readout of the stored data commences, the calibration sequence is inhibited because it could prevent the collection of 150 seconds of real-time data during a flare.

When calibration data are being stored in the memory, the seven range bits of the primary group are not used to indicate range. They are used to clearly indicate that calibration data are being stored and to identify the *A* or *B* detectors as the source of stored data from experiments 1, 3, 4, 10, and 12. Although this information only appears with calibration data in the memory, it is readily available from the real-time data. The stored data have no way to indicate whether the linear or the logarithmic electrometer-amplifier is being used for experiment 12. This information must be obtained from the

real-time data or from command records. Calibration data from secondary group S1 are never stored in the memory. Data from the S2 and S3 secondary groups are stored on alternate calibrations.

Stored data are normally transmitted by the TM 2 transmitter by ground command. If the TM 2 transmitter fails, the stored data can be transmitted by the TM 1 transmitter operating in either the analog or digital mode. Analog mode transmission of the stored data uses IRIG channel 12. Use of the TM 1 transmitter in the digital mode would temporarily interrupt the transmission of all real-time data. Use of the TM 1 transmitter in the analog mode would temporarily interrupt the transmission of real-time PCM data but would not interfere with the transmission of real-time analog data.

Stellrad Data Transmission

Since the power consumption of the Stellrad experiment is quite large, it is turned on only over a ground station and its data are transmitted in real-time only. The Stellrad experiment data are normally transmitted by the TM 2 transmitter. In case of failure of the TM 2 transmitter the Stellrad experiment data can also be transmitted by the TM 1 transmitter operating in a digital mode. This would temporarily interrupt the transmission of real-time solar experiment data.

DATA REDUCTION

X-Ray Experiments

The response of an ionization chamber to radiation of a given wavelength is determined by the detector window material and thickness and the gas used to fill the detector. In the case of x-ray detectors, such as those used on experiments 1 through 6, 10, and 13 of SOLRAD 10, the window completely absorbs low-energy radiation and provides a long-wavelength limit to the detector's sensitivity. The gas filling of the detector is transparent to high-energy radiation which provides a short-wavelength limit to the detector's sensitivity. Radiation whose wavelength is between the two sensitivity limits for the detector will be only partially absorbed by the window material and that portion which penetrates the window will interact with the filling gas. The interaction between the radiation and the gas produces electron-ion pairs in the gas. The number of pairs produced per unit energy of the radiation is a characteristic of the type of gas used. The electrons and ions move, under the influence of an applied electric field, to the anode and cathode respectively, producing a current whose magnitude can be related to the energy flux incident upon the detector window. The detector geometry, electrode configuration, and applied potential are designed to provide a detector with a fast response and to insure that the electron-ion pairs produced by the incident radiation do not cause secondary ionization or recombine before reaching the electrodes.

The current generated in an ionization chamber is given by

$$I = e\omega A \int_0^{\infty} E(\lambda)\epsilon(\lambda) d\lambda, \quad (2)$$

where e is the electronic charge, ω is the number of ion pairs produced in the gas per unit energy of the incident photon, A is the effective window area of the detector, $E(\lambda)$ is the solar emission spectrum, $\epsilon(\lambda)$ is the efficiency of the detector, and λ is wavelength. For actual calculations, the integration limits are determined by the range of wavelengths over which the detector's efficiency is nonzero.

The detector's efficiency is given by

$$\epsilon(\lambda) = \exp \left[- \sum_i (\mu_m \rho x)_i \right] \left\{ 1 - \exp \left[- \sum_j (\mu_m \rho x)_j \right] \right\}, \quad (3)$$

where the mass absorption coefficients μ_m are wavelength dependent and the area densities ρx are functions of material and geometry. The first exponential summation gives the fraction of incident radiation of wavelength λ which penetrates the solid window and the small volume of gas immediately behind the window where electron-ion pairs formed will not be collected by the electrodes before recombination occurs. The summation over i is a summation over all of the elements which make up the window material and filling gas. The quantity in braces gives the fraction of radiation which interacts with the gas to form electron-ion pairs which are collected by the electrodes. The summation over j is a summation over all of the elements which make up the filling gas.

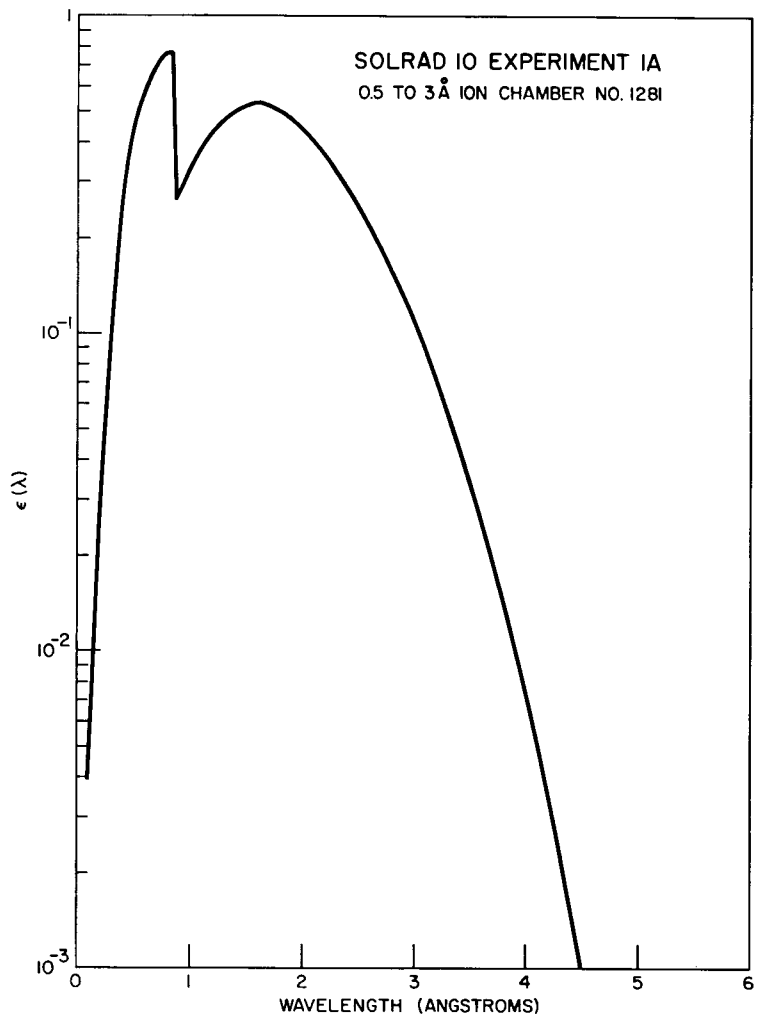
Figures 5(a) through 5(l) show the efficiency of the SOLRAD 10 x-ray experiments as a function of wavelength. The values of area density ρx used in calculating detector efficiency are given in Table 1. The mass absorption coefficients $\mu_m(\lambda)$ used were obtained from Henke et al. (2), McGuire (3), Guttmann and Wagenfeld (4), and McCrary et al. (5). The data from these sources were approximated by a least-squares fit of the form

$$\ln \mu_m = \sum_{k=0}^4 a_k (\ln \lambda)^k \quad (4)$$

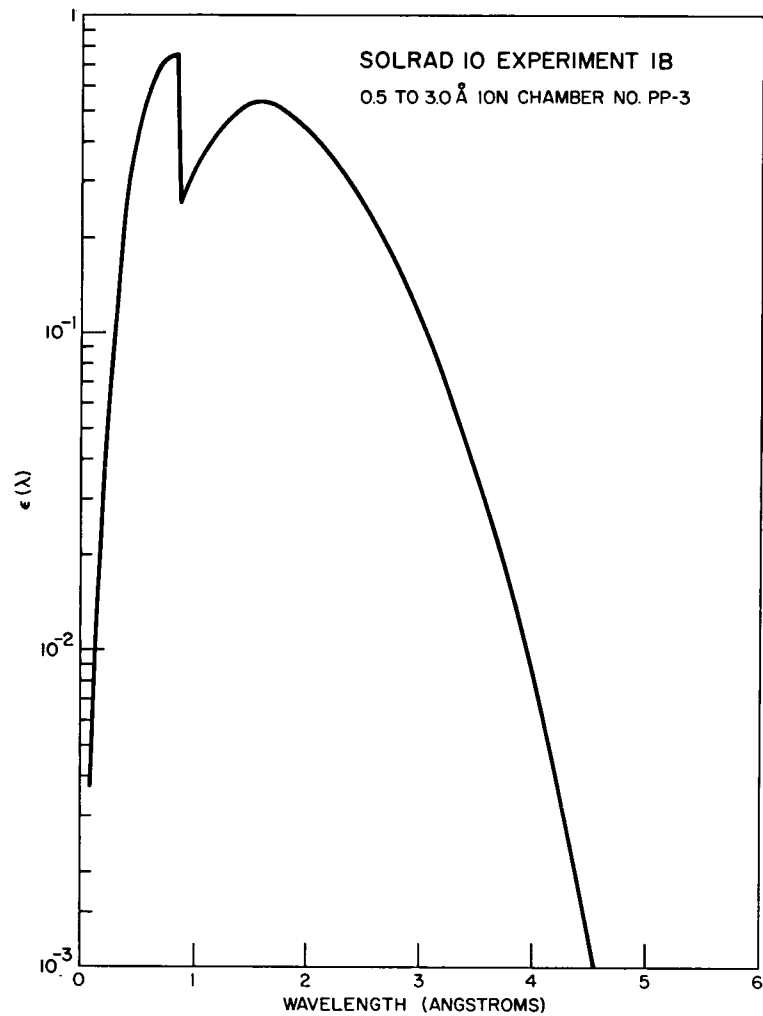
with μ_m in units of cm^2/g and λ in angstroms. The values of the coefficients a_k , along with their wavelength range of validity, are presented in Table 6.

On all NRL x-ray experiments prior to those on SOLRAD 10, the mass absorption coefficients were calculated using a method given by Henke et al. (6). For all experiments except experiment 4 the efficiencies calculated using the new and the old mass absorption coefficients differed by less than 10 percent. However, in the case of experiment 4, the use of the more recent mass absorption coefficients produced an efficiency 1.43 times larger than that obtained using the older coefficients. Therefore, to compare the experiment 4 data of SOLRAD 10 with similar data from earlier experiments, the SOLRAD 10 data must be multiplied by 0.70.

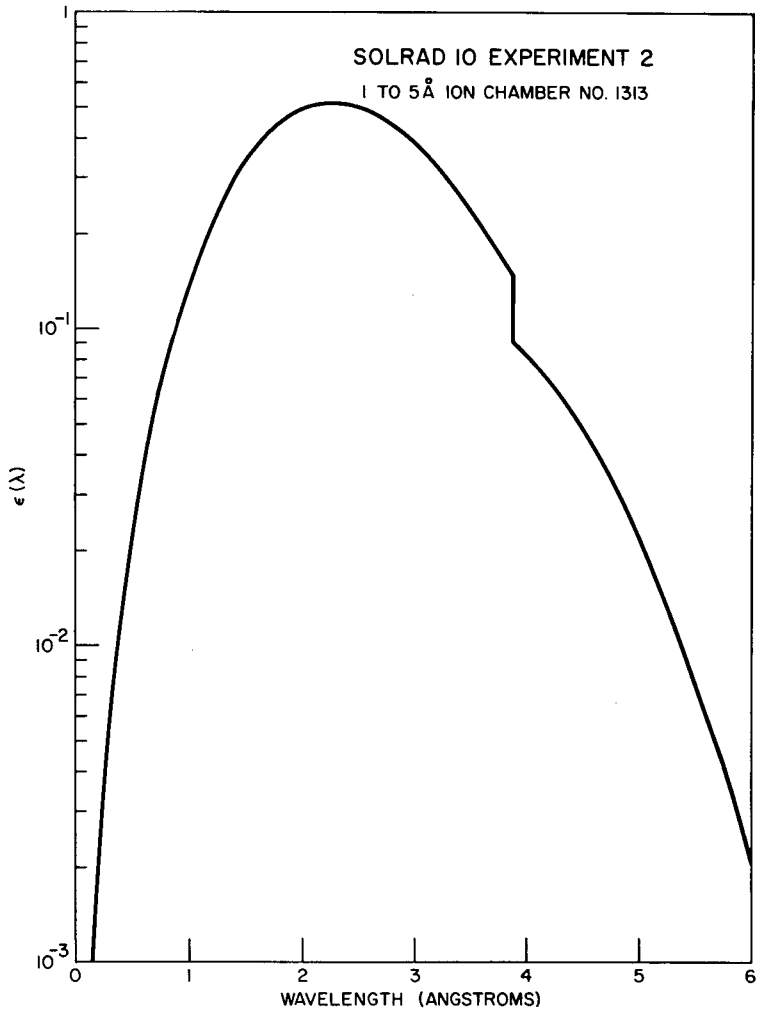
Since the solar emission spectrum $E(\lambda)$ is not accurately known in the x-ray region (and even if it were known, it would be extremely time dependent), a simple solar emission model is assumed and an equation appropriate to that model is used to represent the solar emission spectrum. The most frequently used emission models assume that the solar x-ray emission is entirely due to one mechanism — either free-free electron transitions



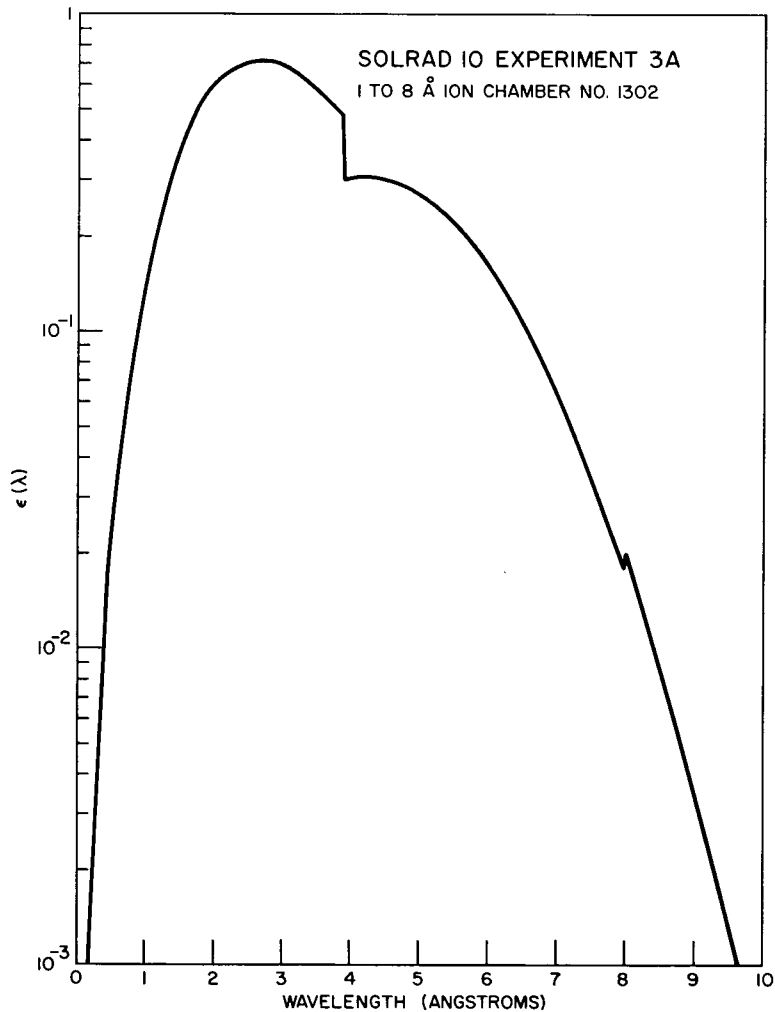
(a) Experiment 1A



(b) Experiment 1B

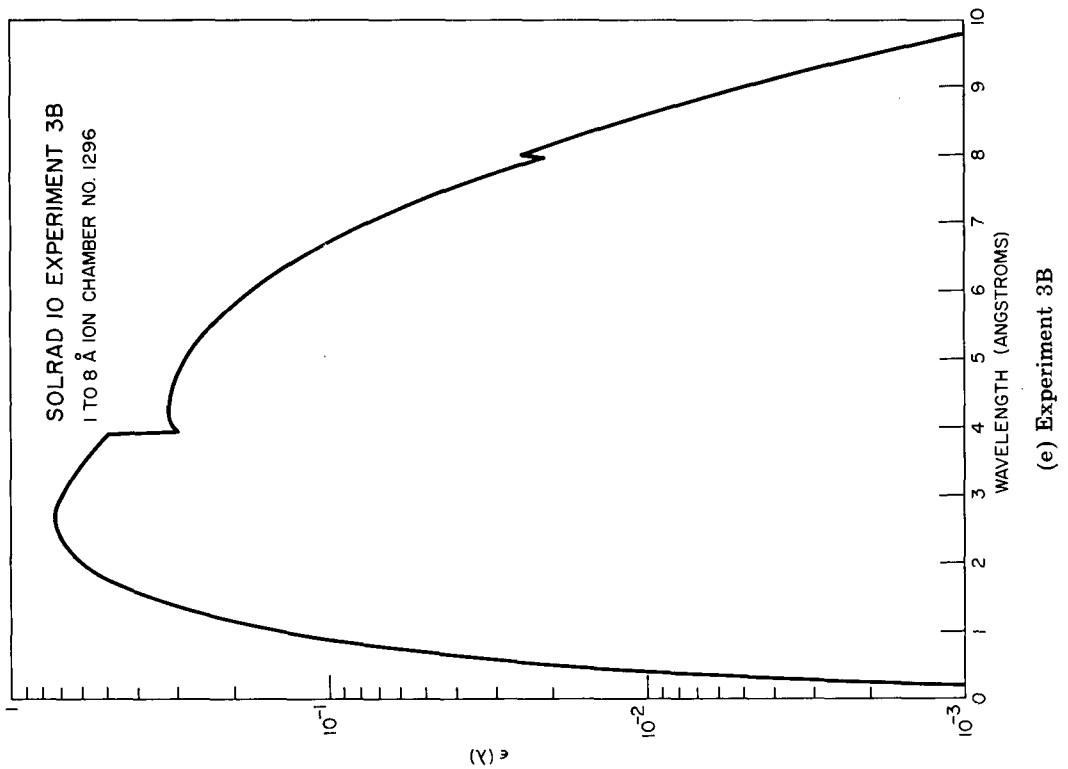
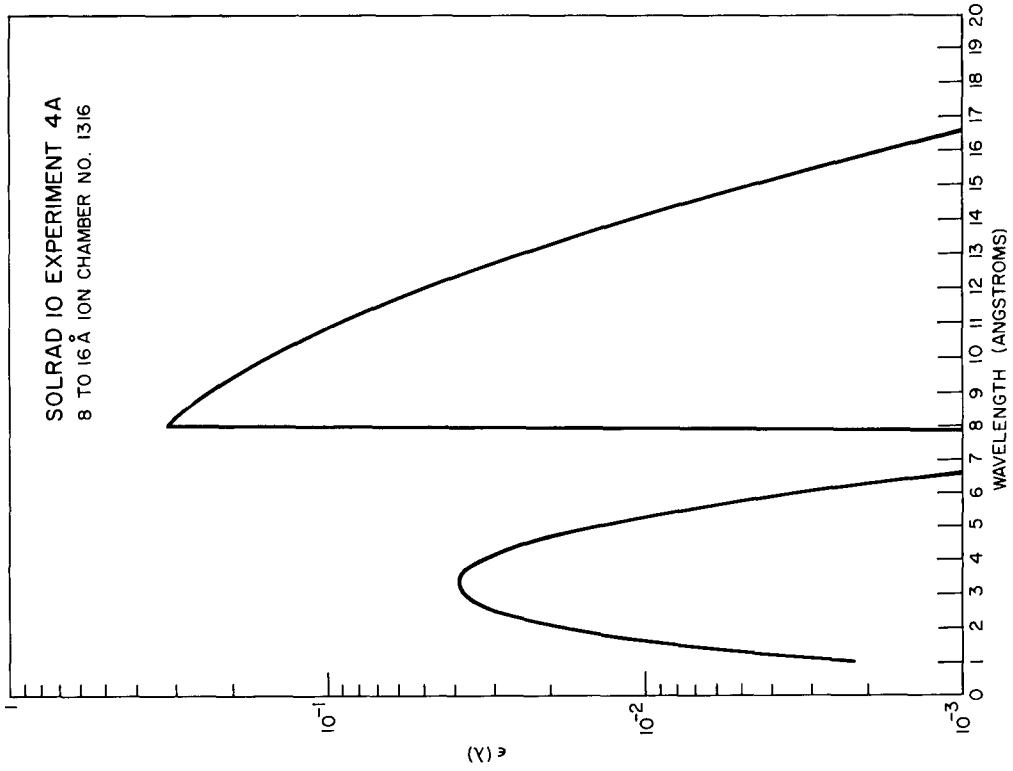


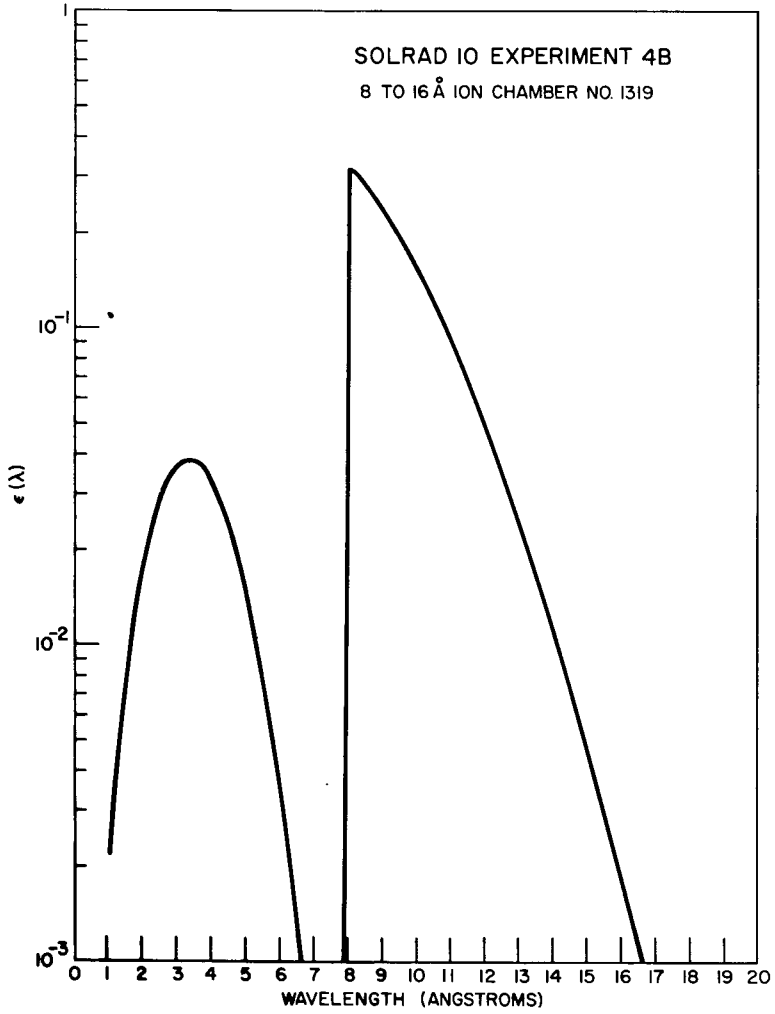
(c) Experiment 2



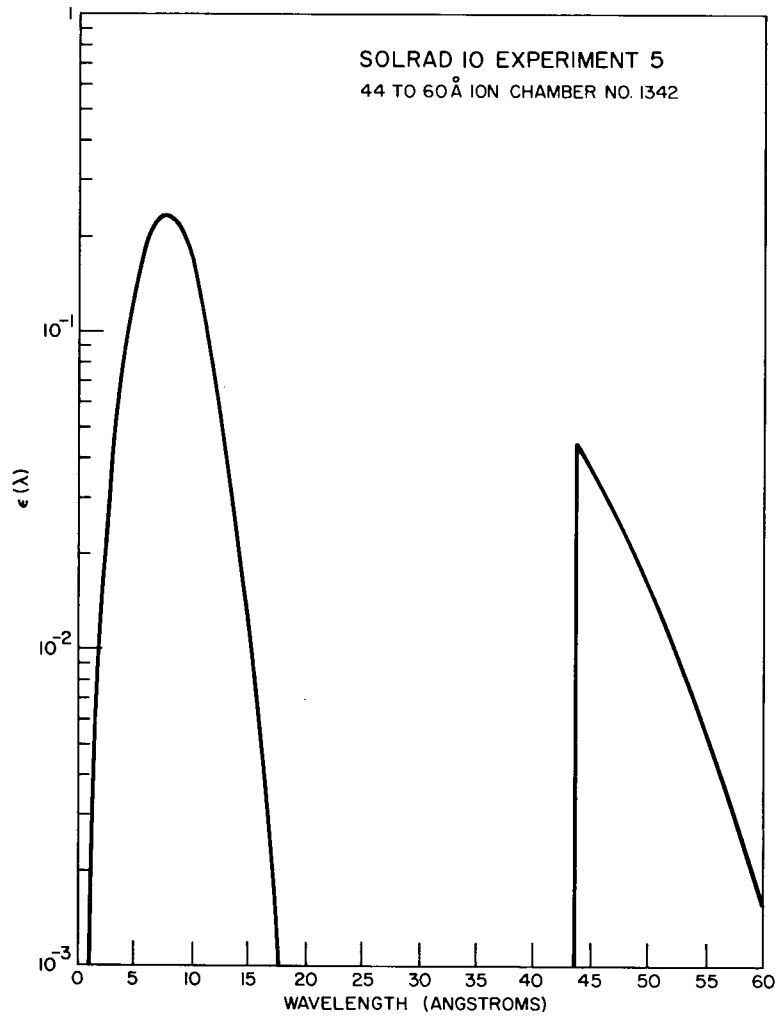
(d) Experiment 3A

Fig. 5 — Detector efficiency as a function of wavelength



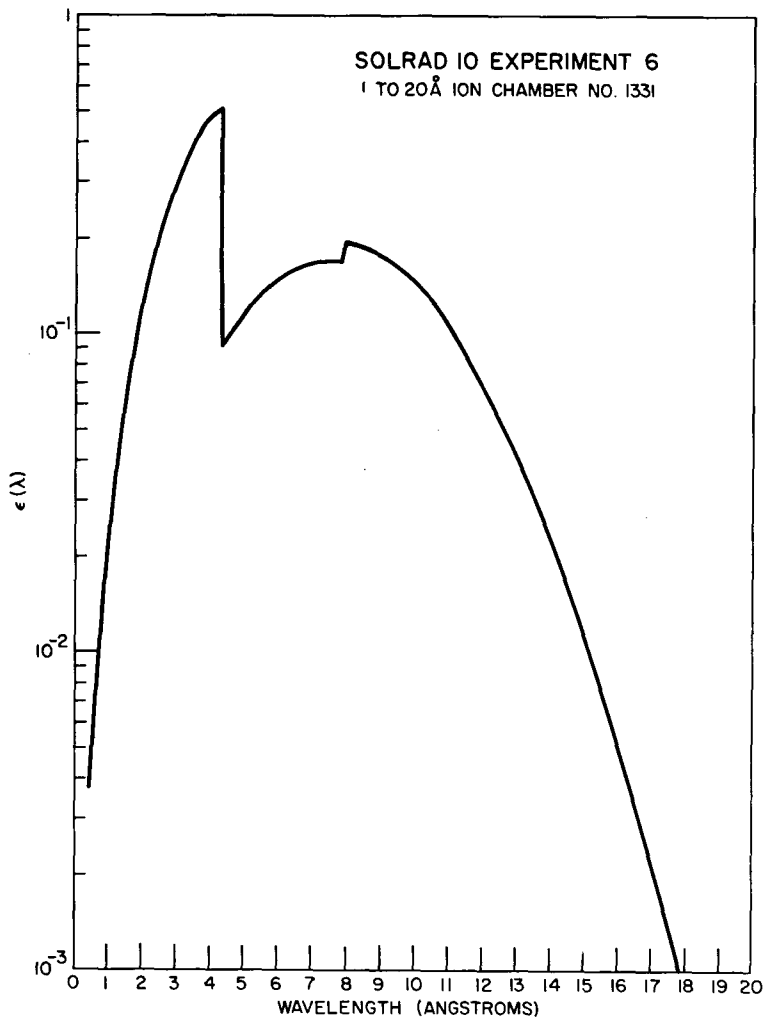


(g) Experiment 4B

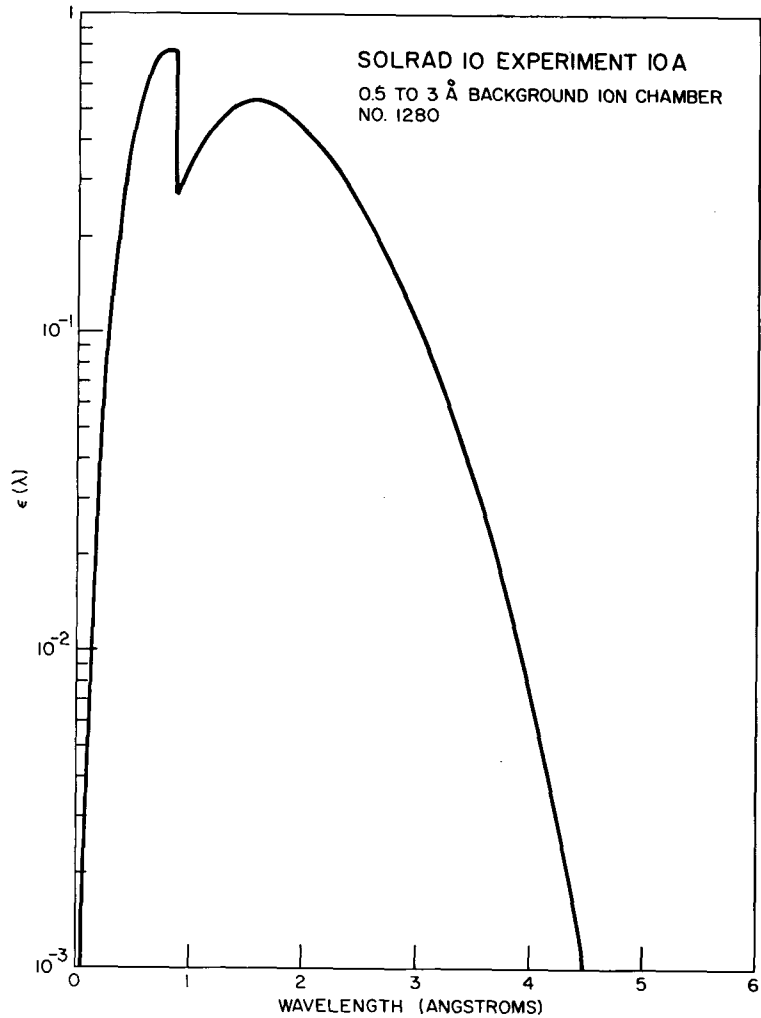


(h) Experiment 5

Fig. 5 (Continued) — Detector efficiency as a function of wavelength



(i) Experiment 6



(j) Experiment 10A

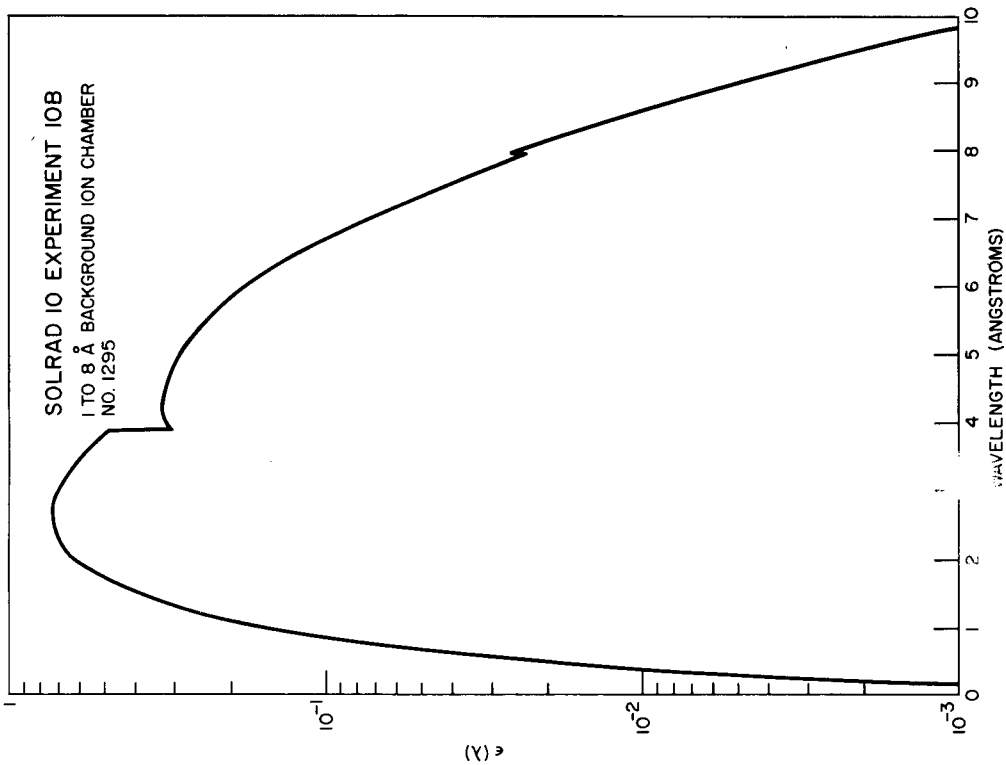
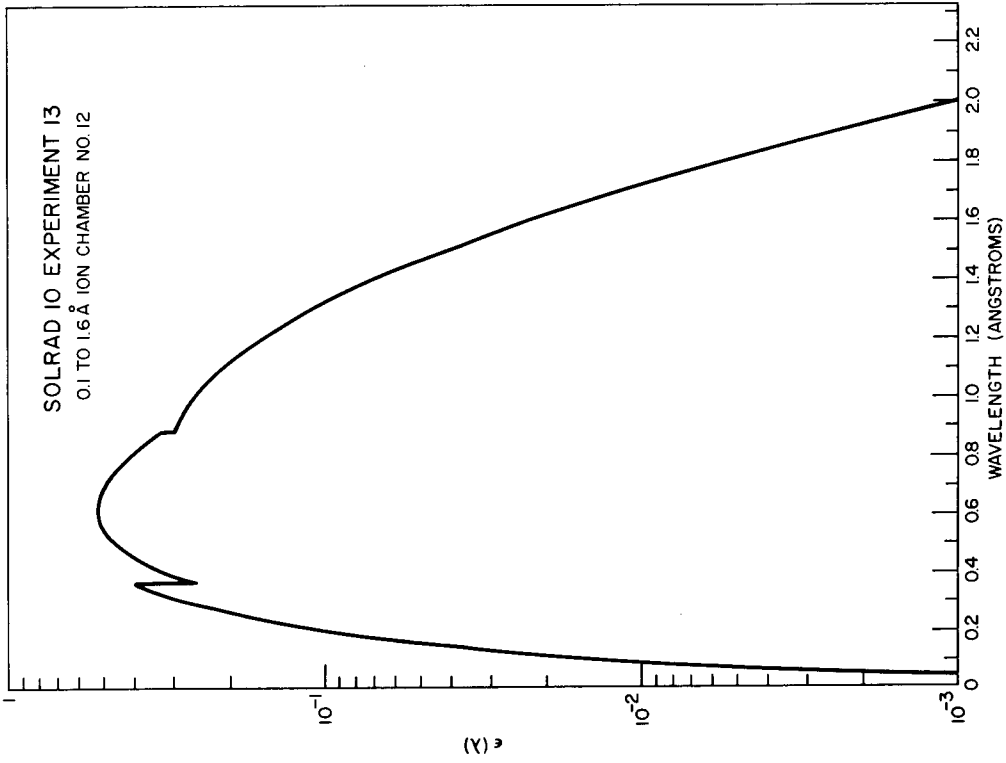


Fig. 5 (Continued) — Detector efficiency as a function of wavelength

Table 6
Coefficients Relating $\ln \mu_m$ to $\ln \lambda$

| Material (Validity Range) | a_0 | a_1 | a_2 | a_3 | a_4 |
|---------------------------------------|----------|---------|------------|-----------|-----------|
| Aluminum (0.00 — 7.952 Å) | 2.621 | 2.966 | 0.04802 | - 0.1192 | 0.02347 |
| Aluminum (7.952 — 44.00 Å) | - 7.558 | 10.88 | - 2.763 | 0.2972 | 0.0000 |
| Argon (0.10 — 3.871 Å) | 3.539 | 2.869 | 0.0000 | 0.0000 | 0.0000 |
| Argon (3.871 — 43.192 Å) | 3.735 | - 2.033 | 3.312 | - 0.9724 | 0.09955 |
| Beryllium (0.00 — 44.00 Å) | - 0.5090 | 1.839 | 0.5023 | - 0.03674 | - 0.01034 |
| CCl ₄ (0.50 — 4.397 Å) | 3.482 | 2.628 | 0.03754 | 0.0000 | 0.0000 |
| CCl ₄ (4.397 — 40.00 Å) | 2.440 | 0.8846 | 0.8624 | - 0.1351 | 0.0000 |
| Krypton (0.10 — 0.866 Å) | 5.660 | 3.187 | 0.0000 | 0.0000 | 0.0000 |
| Krypton (0.866 — 6.47 Å) | 3.256 | 2.498 | 0.9860 | - 1.108 | 0.3151 |
| Mylar (0.5 — 23.301 Å) | 0.4794 | 3.137 | - 0.004678 | - 0.02285 | 0.0000 |
| Mylar (23.301 — 43.648 Å) | - 1.710 | 4.198 | - 0.2570 | 0.0000 | 0.0000 |
| Mylar (43.648 — 70.00 Å) | - 0.9863 | 2.407 | 0.0000 | 0.0000 | 0.0000 |
| Nitrogen (0.00 — 30.99 Å) | 0.2828 | 3.546 | - 0.1740 | 0.0000 | 0.0000 |
| Nitrogen (30.99 — 114.00 Å) | 0.5779 | 1.718 | 0.07978 | 0.0000 | 0.0000 |
| Xenon (0.00 — 0.358 Å) | 6.382 | 2.768 | 0.0000 | 0.0000 | 0.0000 |
| Xenon (0.358 — 2.30 Å) | 4.363 | 2.538 | 0.02286 | 0.3182 | 0.0000 |
| Xenon (2.30 — 11.02 Å) | 1.216 | 4.857 | - 0.6978 | 0.0000 | 0.0000 |

(bremsstrahlung) or dilute blackbody emission. Both mechanisms are temperature dependent. A dilute blackbody (graybody) solar emission spectrum is assumed when reducing x-ray data from NRL experiments (7).

Under the graybody assumption, the energy per unit wavelength interval is given by

$$E(\lambda, T) = B\lambda^{-5} [\exp(\alpha/T\lambda) - 1]^{-1} \quad (5)$$

with $B = 2\pi hc^2 D$ and $\alpha = hc/k$, where h is Planck's constant, c is the speed of light, k is Boltzmann's constant, T is the color temperature of the emitting medium, and D is a dilution factor which indicates the amount by which the solar emission intensity falls below that expected from a true blackbody radiator at the temperature T . The value of B (or D) for any color temperature T can be obtained by comparing the current generated in the detector by solar x rays (I_x) with the calculated value of

$$I'(T) = ewA \int_{\lambda_1}^{\lambda_2} \epsilon(\lambda)\lambda^{-5} [\exp(\alpha/T\lambda) - 1]^{-1} d\lambda, \text{ i.e., } \frac{I_x}{I'(T)} = B(T). \quad (6)$$

Since the solar spectrum over the entire x-ray region of interest, 0.1 to 60 Å, cannot be adequately approximated by a graybody spectrum for a single color temperature, the x-ray spectrum is divided into segments corresponding to the sensitive bands of the detectors, and appropriate color temperatures are selected for each spectral segment. The relationship between the solar energy flux (ergs/cm²sec) in such a spectral segment and the current generated in the detector is

$$F = \frac{I \int_{\lambda_a}^{\lambda_b} E(\lambda, T) d\lambda}{eA\omega \int_{\lambda_1}^{\lambda_2} \epsilon(\lambda)E(\lambda, T) d\lambda} = \frac{I}{A} K(T). \quad (7)$$

The integration limits λ_a and λ_b define the bounds of the band whose energy flux is being calculated and are generally different from the limits λ_1 and λ_2 . The latter limits are determined from the wavelength range over which the detector's efficiency is nonzero. Table 7 shows typical values for the four integration limits for the SOLRAD 10 x-ray experiments.

To facilitate automatic processing of the large amount of data produced by the experiments, all data from a given detector, whether obtained during a solar flare or a lull in solar activity, will be reduced using the same color temperature. The selected temperatures are shown in Table 2. This approach is consistent with the choice of a graybody spectrum to approximate the solar spectrum. Neither approach has a basis in the present knowledge of solar physics, but both are extremely useful simplifications when processing large quantities of data (see Appendix B).

The telemetered experiment data are actually a measure of the voltage levels produced in the electrometer-amplifier by the current generated in the detector. In the case of the

Table 7
Integration Limits for Detector
Current-to-Flux Calculations

| Experiment | $\lambda_a(\text{\AA})$ | $\lambda_b(\text{\AA})$ | $\lambda_1(\text{\AA})$ | $\lambda_2(\text{\AA})$ |
|------------|-------------------------|-------------------------|-------------------------|-------------------------|
| 1 | 0.5 | 3.0 | 0.1 | 6.4 |
| 2 | 1.0 | 5.0 | 0.1 | 10.0 |
| 3 | 1.0 | 8.0 | 0.1 | 12.0 |
| 4 | 8.0 | 20.0 | 1.0 | 25.0 |
| 5 | 44.0 | 60.0 | 0.5 | 70.0 |
| 6 | 1.0 | 20.0 | 0.5 | 30.0 |
| 13 | 0.1 | 1.6 | 0.01 | 3.20 |

linear electrometer-amplifiers used with the x-ray experiments, the voltage output is related to the detector current by

$$V = m_i I + b_i, \quad (8)$$

where m_i and b_i are the slope and intercept, respectively, for range i . Therefore, the conversion from telemetered voltage levels to solar energy flux is accomplished by

$$F = \frac{K(T) (V - b_i)}{A m_i} = C(V - b_i). \quad (9)$$

Values for A , m_i , b_i , K , T , and C for the x-ray experiments are given in Table 2. Figure 6 shows the ranges of energy flux measurable by the x-ray experiments, based on the current-to-flux calculations described above.

Experiment 11 uses a scintillating crystal, a photomultiplier, and pulse-height analysis to detect x rays and measure their energy. The energy of x rays absorbed in the crystal is converted to visible light which generates a pulse in the photomultiplier. The magnitude of the photomultiplier pulse is an approximate measure of the x-ray energy deposited in the crystal. The efficiency curve of this experiment is determined by the filtering materials which lie between the source and the crystal and by the material and thickness of the crystal. The low-energy (longer-wavelength) sensitivity limit is caused by absorption of x rays by the following filters: a thermal blanket of approximately 0.05 cm Mylar, a 0.05-cm-thick aluminum window, a 0.01-cm-thick beryllium window, a coating of titanium dioxide reflecting paint approximately 0.03 cm thick, and approximately 0.13 cm of plastic (polyvinyltoluene). The high-energy (short-wavelength) sensitivity limit is determined by the thickness of the CsI crystal — 1.0 cm. Figure 7 displays the efficiency of experiment 11 as a function of x-ray energy between 10 and 70 keV. The efficiency above 70 keV is not shown but is approximately 0.9 at 200 keV and approximately 0.8 at 250 keV.

The correspondence between x-ray photon energy and photomultiplier pulse height is not exact. X-ray emission at a precise wavelength — line emission — produces pulse heights having an approximately Gaussian distribution. For experiment 11, the full-width-at-half-maximum of the distribution, i.e., the resolution, is about 0.50 at 22 keV, 0.30 at

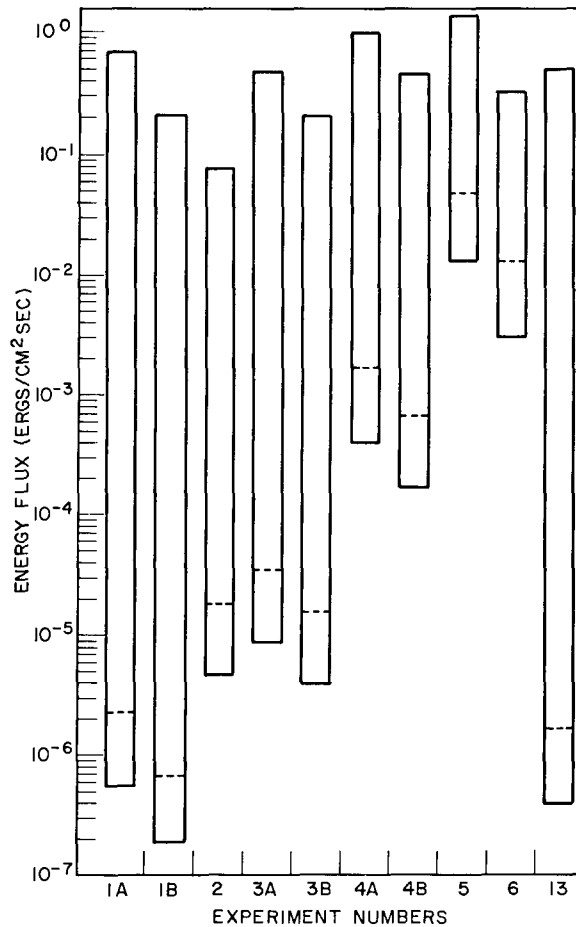


Fig. 6 — Dynamic ranges of the SOLRAD 10 x-ray experiments. The conversion from detector current to solar energy flux assumes a gray-body solar emission spectrum at a constant color temperature. The dashed lines indicate the sensitivity threshold for memory data, and the solid lines are accurate for PCM real-time data.

60 keV, and 0.25 at 125 keV. The americium 241 calibration source, which emits 60 keV x rays, is used in flight to verify the stability of the resolution.

The four channels of the pulse-height analyzer were originally set to sort into the following energy ranges: 15 to 20, 20 to 30, 30 to 60, and 60 to 150 keV. However, until early September 1971, the system gain drifted from the initial setting. The gain has been stable since that time and the present limits of the four energy channels are approximately 21 to 28, 28 to 42, 42 to 84, and 84 to 210 keV.

Ultraviolet Experiments

Ionization chambers used to measure ultraviolet radiation are essentially similar in operation to the x-ray sensors except that the roles of the window material and the filler gas are reversed in determining the upper and lower response limits. In the case of ultraviolet detectors, such as those used for experiments 7 through 9 of SOLRAD 10, the

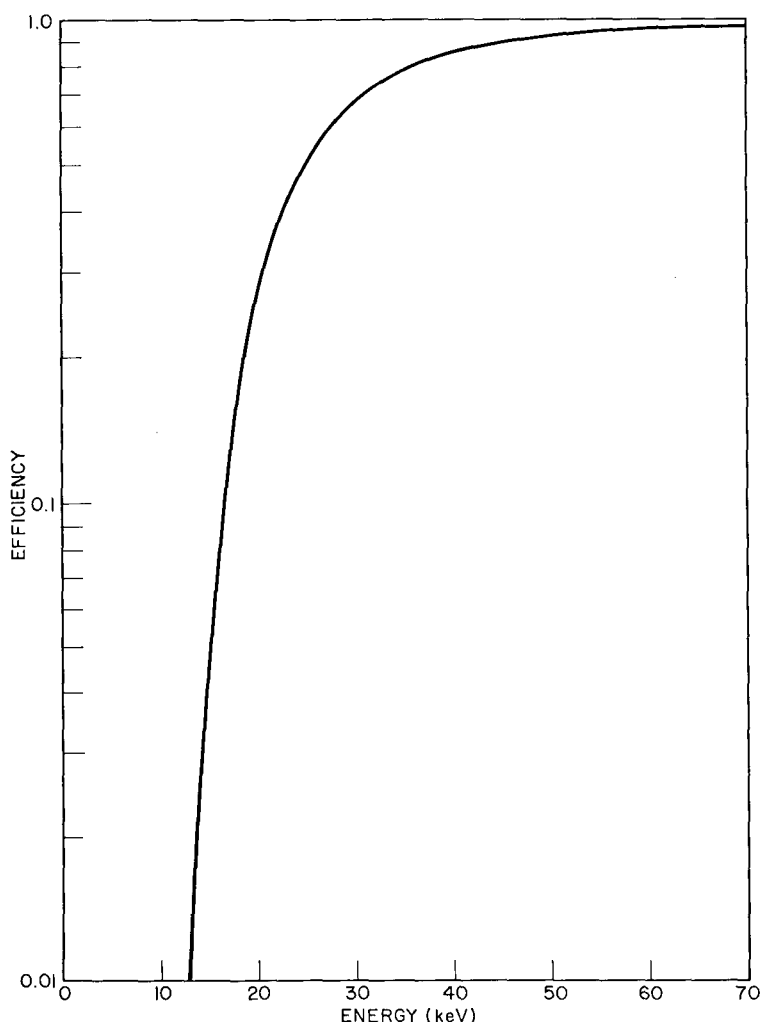


Fig. 7 — Efficiency as a function of x-ray energy for experiment 11

transmittance characteristics of the window material determine the short-wavelength response limit. The photoionization of the gas defines the long-wavelength response limit.

To relate the telemetered voltage values to the solar ultraviolet energy flux incident on the detector's window, the current generated in the detector per unit of incident energy flux must be determined. As a starting point in this procedure, the quantum efficiency of the detector is determined. The quantum efficiency is a measure of the number of electrons which will result from ionization caused by one incident photon. Since the nominal 1080 to 1350 Å response band of experiment 7 is strongly dominated by the hydrogen Lyman-alpha line at 1216 Å, the measurement of the detectors' quantum efficiencies assumes that all radiation in the response band is concentrated at 1216 Å. The quantum efficiency values used for the detectors for experiments 8 and 9 are averaged quantum efficiencies obtained from the plots shown in Fig. 8. The displayed plot for experiment 8 was obtained by using measured quantum efficiency values for the flight

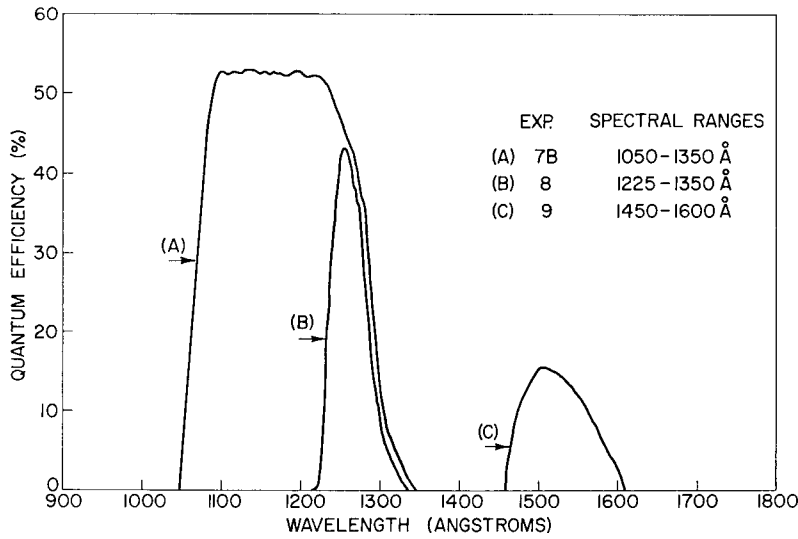


Fig. 8 — Detector efficiency as a function of wavelength for experiments 7 through 9

detector to normalize a curve whose general shape was determined by the calcium fluoride and nitric oxide responses at the limits of the response band. The displayed plot for experiment 9 was obtained by measuring the quantum efficiency of the flight detector at 15 points over the response band.

Since an average quantum efficiency is used to represent each response band for experiments 8 and 9, the energy carried by an average photon in these bands must be used. A flat emission spectrum over the band is assumed in calculating the average photon energy. The current generated in the detector is given by

$$I = \left(\frac{AF}{Y}\right)(NQ), \tag{10}$$

where Q is the quantum efficiency, Y is the average energy per photon, N is the number of coulombs per electronic charge, 1.60×10^{-19} , A is the window area, and F is the solar flux (ergs/cm²sec). Then F can be expressed as

$$F = \left(\frac{Y}{NQ}\right)\frac{I}{A}, \tag{11}$$

and we can set

$$K = \left(\frac{Y}{NQ}\right), \tag{12}$$

where K is a detector conversion constant as in the case of the x-ray sensors. Therefore, we can relate the telemetered voltage to the incident ultraviolet flux by

$$F = \frac{K(V - b)}{mA} = C(V - b) \tag{13}$$

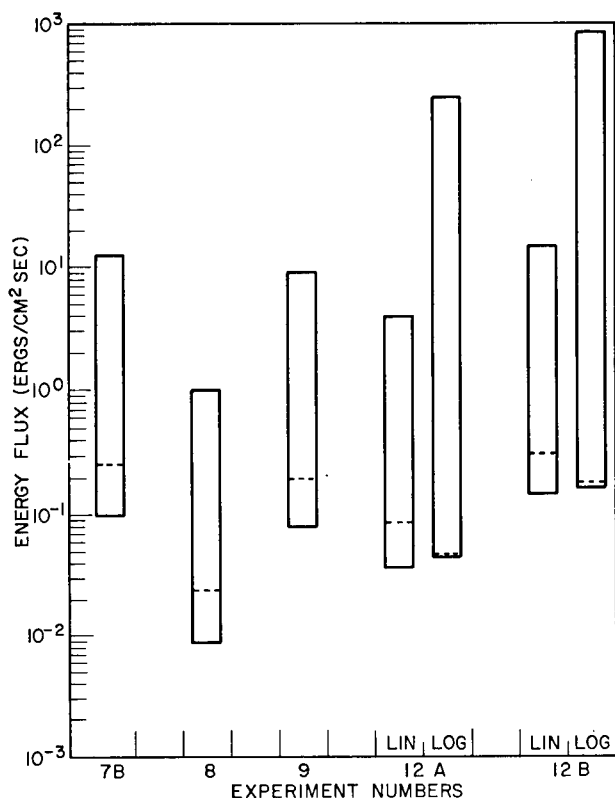


Fig. 9 — Dynamic ranges of the SOLRAD 10 ultraviolet and extreme ultraviolet experiments. The dashed lines indicate the sensitivity threshold for memory data, and the solid lines are accurate for PCM real-time data.

just as we did with the x-ray sensors. The values used for K , b , m , A , and C are given in Table 2 and values for Q are given in Table 1. Figure 9 shows the ranges of energy flux measurable by the ultraviolet experiments based on the current-to-flux calculations described above.

Extreme Ultraviolet Experiment

The sensors used to measure the solar radiation in the 170 to 700 Å band of the extreme ultraviolet spectrum, experiment 12, use a negatively biased photosensitive surface to generate a current. Photons striking the 2000 Å thick lithium fluoride surface layer cause a number of electrons to be emitted from the surface. The number of electrons ejected per incident photon, the quantum efficiency of the surface, is a function of the energy of the photon. A positively biased filter placed in front of the emitting surface collects the emitted electrons, and, as in the case of the ionization chambers, an electrometer-amplifier converts the generated current to a voltage level. The efficiency curves for the detector and filter combinations as presented in Fig. 10 were obtained from the lithium fluoride quantum efficiency curve and the transmittance curves for aluminum and carbon presented by Samson (8) and the aluminum oxide transmittance curve given by Burton (9). The detectors' response to wavelengths less than 170 Å is ignored because of the relatively small amount of flux below that wavelength.

The detector conversion constant K was obtained by folding the extreme ultraviolet spectrum given by Hinteregger (10) into the detectors' response curves. When the linear

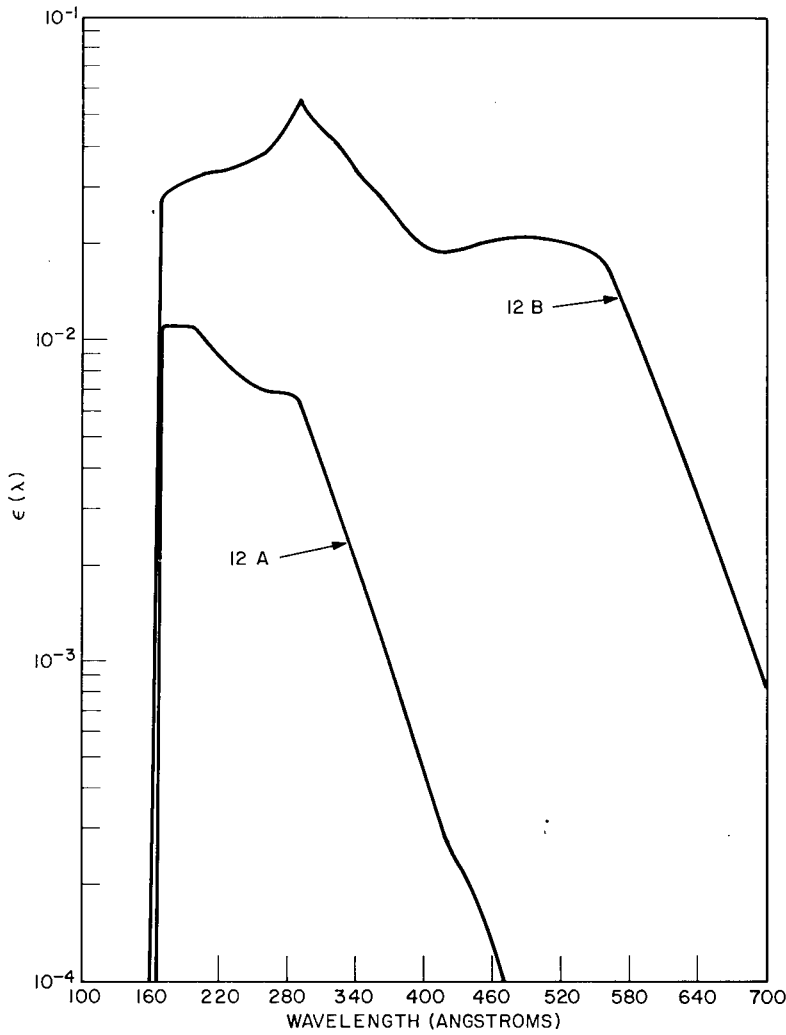


Fig. 10 — Detector efficiency as a function of wavelength for experiment 12

electrometer-amplifier is used, the telemetered voltage levels can be converted to energy flux values using

$$F = \frac{K(V - b)}{mA} = C(V - b). \tag{14}$$

However, since the voltage-vs-current expression for the logarithmic amplifier is of the form

$$V = m (\log_{10} I) + b, \tag{15}$$

the conversion from telemetered voltage to energy flux for the logarithmic amplifier uses

$$\log_{10} F = C + (V - b)/m. \tag{16}$$

Values for C , K , m , b , and A for experiment 12 are given in Table 2 and information about the filter materials and thicknesses used in the detectors is given in Table 1. Figure 9 shows the range of the energy flux measurable by this experiment based on the current-to-flux calculations described.

SATELLITE ORIENTATION CONTROL

Spin and Attitude Control Systems

SOLRAD 10 is a spin-stabilized satellite which must be oriented with its spin axis toward the sun if it is to carry out its solar monitoring mission. The spin rate is maintained at a nominal 60 rpm by the spin control. The attitude control holds the angle between the spin axis and the satellite-sun line, the aspect angle, within a selected value. If a failure occurs in the spin control, SOLRAD 10 would remain stable for several weeks, or even months, while the spin rate decayed. However, if the attitude control fails, the continuous change in aspect angle due to the motion of the Earth around the sun would cause the sun to be removed from the field of view of the collimated solar experiments in a few days. Therefore, a great amount of redundancy was built into the spin and attitude controls.

There are a total of seven control systems aboard the satellite — three for spin control and four for attitude control. The seven control systems can also be divided into two main groups based on the fuel used — liquid anhydrous ammonia or liquid hydrazine. All ammonia systems are fueled from a common tank and all hydrazine systems are fueled from a common tank. Except for their fuel sources, the seven control systems are completely independent.

Two of the spin control systems use liquid ammonia for fuel. The third spin control system is fueled with liquid hydrazine. When it is necessary to increase the satellite's spin rate, one of the three systems is activated by ground command. There is no automatic mode of operation for the spin control.

Two of the four attitude control systems are fueled by hydrazine and two by ammonia. One of the four attitude control systems is selected by ground-command and put into a mode in which it is able to respond to firing pulses generated by ground command or automatically based on satellite-borne aspect angle sensors and automatic control electronics. There are two types of aspect angle sensors aboard the satellite — wide angle and fine angle. Two of each type of sensors are carried for redundancy, and each of the four sensors has its own automatic control electronics. One of the two wide-angle sensors is selected by ground command whenever the aspect angle exceeds 5° . One of the two fine-angle sensors is used when the aspect angle is less than 5° , which should be the normal condition. When a fine-angle sensor is in use, the automatic control electronics will generate firing pulses whenever the aspect angle exceeds a control angle selected by ground command from the following four choices: 0.5° , 1° , 2° , or 4° . When a wide-angle sensor is in use, firing pulses will be continually generated by the automatic control electronics until the aspect angle is less than 5° .

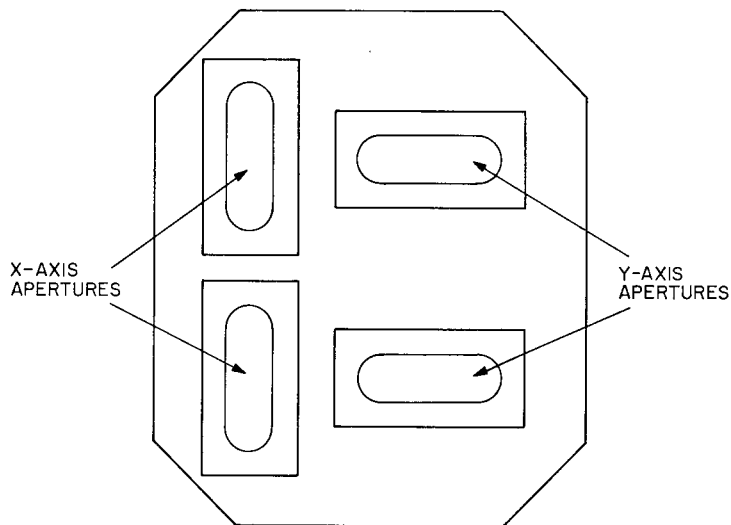


Fig. 11 — Arrangement of apertures for fine-angle attitude control sensors. Their location on the solar-oriented surface of SOLRAD 10 can be seen in Fig. 2.

Aspect Sensor Data Transmission

Each of the two fine-angle sensors is made up of four components. Each of the components is two segments of solar cell cut to obtain a sensitive area of 0.5 inch by 0.69 inch. These components are paired and wired differentially to form one-half of a fine-angle sensor. The two halves of a fine-angle sensor are mounted so that their long axes form a 90° angle. One of the sensor halves is labeled "x-axis sensor" and the other half is called the "y-axis sensor." Figure 11 shows the arrangement of the components of the two fine-angle sensors.

Each of the sensor halves is recessed 2 inches behind an aperture. If the optical axis of the sensor half and its aperture is parallel to the satellite's spin axis, the two components of the sensor half will be equally illuminated by the sun at zero aspect angle. The two components of each sensor half are connected to a differential amplifier which produces an output voltage proportional to the difference in illumination of the two components. If the aspect angle is not zero, the two components of the sensor half will not be equally illuminated, and the differential amplifier will produce a voltage output. As the satellite rotates about its spin axis, the aperture shadow will move around the two components of the sensor half, and the differential amplifier will produce a sinusoidal voltage output. The absolute values of the positive and negative peak voltages for the x axis and y axis are transmitted as real-time PCM data. If the optical axis of a sensor half and its aperture is not parallel to the spin axis of the satellite, there will be a dc offset voltage. The values of these offset voltages for the x and y axis are also included in the PCM telemetry. A direct measurement of the output of the components of the sensor halves never appears in the telemetry. The telemetry carries only a measurement of the difference in output of a pair of components.

As in the case of the fine-angle sensors, a differential output from one of the wide-angle sensors is related to the aspect angle. Therefore, the PCM and analog real-time telemetry carry values of this differential voltage, but the absolute output value of an individual sensor is never transmitted.

ACKNOWLEDGMENTS

The success of a major program such as SOLRAD depends on the efforts of many individuals. Among those who contributed to the preparation and launch of SOLRAD 10 are: E. W. Peterkin, SOLRAD Program Technical Manager; P. G. Wilhelm and the members of the Satellite Techniques Branch of the Space Systems Division; G. Leavitt and his associates in the Electronic Engineering Branch of the Engineering Services Division; and C. H. Chrisman and the members of the Data Systems Branch of the Space Systems Division. E. T. Byram of the Upper Air Physics Branch of the Space Science Division headed the team which prepared the Stellrad Experiment. G. Fritz of the Upper Air Physics Branch prepared experiment 11. R. G. Taylor of the Upper Air Physics Branch was responsible for the flight photometers for the other solar experiments. Experiment 14 was prepared by J. Severns and R. Rovinski of the Satellite Techniques Branch.

REFERENCES

1. R.W. Kreplin and D.M. Horan, "The NRL SOLRAD 9 Satellite — Solar Explorer B — 1968-17A," NRL Report 6800, Mar. 24, 1969.
2. B.L. Henke, R.L. Elgin, R.L. Lent, and R.B. Ledingham, *Norelco Reporter* 14, 112 (1967).
3. E.J. McGuire, *Phys. Rev.* 175, 20 (1968).
4. A.J. Guttmann and H. Wagenfeld, *Acta. Cryst.* 22, 334 (1967).
5. J.H. McCrary, E.H. Plassmann, J.M. Puckett, A.L. Conner, and G.W. Zimmermann, *Phys. Rev.* 153, 307 (1967).
6. B.L. Henke, R. White, and B. Lundberg, *J. Appl. Phys.* 28, 98 (1957).
7. R.W. Kreplin, *Ann. Geophys.* 17, 151 (1961).
8. J.A.R. Samson, *Techniques of Vacuum Ultraviolet Spectroscopy*, Wiley, New York, 1967.
9. W.M. Burton, United Kingdom Atomic Energy Authority Research Group Report CLM-R64, Culham Laboratory, 1966.
10. H.E. Hinteregger, *Ann. Geophys.* 26, 547 (1970).

Appendix A

CORRECTION OF EXPERIMENT 5 DATA FOR RADIATION
WITH WAVELENGTH LESS THAN 20 Å

The efficiency curve for experiment 5 in Fig. 5h clearly shows that the detector is sensitive to x rays with wavelength less than 20 Å, as well as to the 44 to 60 Å band of interest. Experiment 6 is included in the experiment complement of SOLRAD 10 primarily to provide a way to correct the response of experiment 5 for this undesired shorter-wavelength contribution. A description of a technique which may be used to correct the experiment 5 data is provided in this appendix.

The current per unit wavelength produced in the ionization chambers of experiments 5 and 6 is given by

$$\Delta I_j = e\omega_j A_j E(\lambda) \epsilon_j(\lambda) \Delta\lambda, \quad (\text{A1})$$

and the total current generated is given by

$$I_j = e\omega_j A_j \sum_0^{\infty} E(\lambda) \epsilon_j(\lambda) \Delta\lambda. \quad (\text{A2})$$

Experiment 5 will be denoted by the subscript 5 and experiment 6 by the subscript 6. The equations are described in detail in the section titled "X-ray Experiments" in this report.

Since we want to eliminate the current contribution to experiment 5 from wavelengths less than 43.65 Å, let us designate this current by

$$I'_j = e\omega_j A_j \sum_0^{44} E(\lambda) \epsilon_j \Delta\lambda. \quad (\text{A3})$$

We now establish a relationship given by

$$\Delta I_5 = f \Delta I_6, \quad \lambda < 43.65 \text{ Å}, \quad (\text{A4})$$

where f is independent of wavelength. To justify Eq. (A4), the efficiency curves for wavelengths less than 43.65 Å must be considered for both experiments (Figs. 5h and 5i). The efficiency curves in this region must differ because K -absorption edges for Al, Cl, and N are not common to both.

We will consider the range of wavelengths less than 43.65 Å in three separate bands. In the band between 8 and 31 Å, there are no absorption edges which are not common to both detectors, and so we can closely approximate

$$\Delta I_5 = f \Delta I_6, \quad 8 \leq \lambda < 31 \text{ \AA}. \quad (\text{A5})$$

In the band between 31 and 43.65 Å, the detectors have such small efficiency values that

$$\Delta I_5 = f_1 \Delta I_6 = 0, \quad 31 \leq \lambda < 43.65 \text{ \AA}, \quad (\text{A6})$$

and we can immediately set $f_1 = f$. In the band of wavelengths less than 8 Å we can also argue that, for commonly assumed solar emission spectra $E(\lambda, T)$, we will find

$$\Delta I_5 = f_2 \Delta I_6 \approx 0, \quad \lambda < 8 \text{ \AA}, \quad (\text{A7})$$

and we can set $f_2 = f$ without introducing significant error. The current contribution from this band for commonly assumed spectra is extremely small when compared to ΔI_j for the 8 to 31 Å band because the assumed solar emission drops off sharply as the wavelength decreases. This argument will be most valid for wavelengths less than 4.4 Å, where the efficiency curves differ most.

Based on these reasons, we use Eq. (A4) as a reasonable approximation and, since f does not depend on wavelength, we can calculate the value of f by means of

$$f = \frac{\omega_5 A_5 \sum_0^{44} E(\lambda) \epsilon_5(\lambda) \Delta \lambda}{\omega_6 A_6 \sum_0^{44} E(\lambda) \epsilon_6(\lambda) \Delta \lambda}. \quad (\text{A8})$$

If the assumed solar emission spectrum is temperature dependent, $E(\lambda, T)$, then $f = f(T)$. Values of $f(T)$ for selected color temperatures for an assumed graybody spectrum are given in Table A1.

Table A1
Correction Constants for Experiment 5 Data

| T (10^6 K) | $f(T)$ | $K_c(T)$ (erg/sec amp) |
|-----------------------------|--------|---------------------------|
| 0.5 | 0.922 | 2.44×10^{10} |
| 1.0 | 0.942 | 2.01×10^{10} |
| 1.5 | 0.974 | 1.91×10^{10} |
| 2.0 | 1.00 | 1.71×10^{10} |

Now a conversion constant $K_c(T)$ for calculating the 44 to 60 Å flux from the currents generated in the detectors of experiments 5 and 6 must be obtained. This conversion constant will express the relationship between the 44 to 60 Å solar flux striking the window of the experiment 5 detector and the current generated in the detector by radiation with wavelength greater than 43.65 Å. This current due to radiation with wavelength greater than 43.65 Å can be expressed in terms of Eqs. (A2) through (A4) as

$$e\omega_5 A_5 \sum_{44}^{70} E(\lambda, T) \epsilon_5(\lambda) \Delta\lambda = I_5 - I'_5 = I_5 - fI'_6. \quad (\text{A9})$$

For calculations, placing the upper summation limit at 70 Å for experiment 5 includes all nonzero efficiency values. In the case of experiment 6, the upper summation limit of I'_6 , 43.65 Å, is well into the region where the detector efficiency values approach zero for all practical calculations.

Therefore, we can use

$$I_5 - fI'_6 = I_5 - fI_6. \quad (\text{A10})$$

The conversion constant $K_c(T)$ can now be expressed by

$$K_c(T) = \frac{A_5 \sum_{44}^{60} E(\lambda, T) \Delta\lambda}{I_5 - fI_6}, \quad (\text{A11})$$

which can be put in the form

$$K_c(T) = \frac{A_5 \sum_{44}^{60} E(\lambda, T) \Delta\lambda}{eA_5 \omega_5 \sum_0^{70} E(\lambda, T) \epsilon_5(\lambda) \Delta\lambda - eA_6 \omega_6 f(T) \sum_0^{44} E(\lambda, T) \epsilon_6(\lambda) \Delta\lambda}. \quad (\text{A12})$$

Values of $K_c(T)$ based on a graybody emission spectrum for selected color temperatures are given in Table A1.

The corrected flux in the 44 to 60 Å band, F_c , is related to the telemetered voltages for experiments 5 and 6 by

$$\begin{aligned} F_c &= \frac{K_c(T)}{A_5} [I_5 - f(T)I_6] \\ &= \frac{K_c(T)}{A_5} \left[\left(\frac{V_5 - b_5}{m_5} \right) - f(T) \left(\frac{V_6 - b_6}{m_6} \right) \right], \end{aligned} \quad (\text{A13})$$

and to the graybody fluxes by

$$F_c = K_c(T) \left[\frac{F_5}{K_5} - f(T) \frac{F_6}{K_6} \right]. \quad (\text{A14})$$

All subscripts refer to experiment numbers. Values for A , m , b , and K can be obtained from Table 2.

Appendix B

SUBSTITUTING TEMPERATURE-DEPENDENT, BREMSSTRAHLUNG-TYPE SPECTRA FOR GRAYBODY SPECTRA

The use of a graybody solar emission spectrum at a constant color temperature in converting detector current to solar flux values is convenient but not physically realistic. This appendix briefly outlines a method for converting detector current for experiments 1 through 3 to solar flux values based on a more realistic solar emission spectrum. Complete details have been presented in earlier papers.*†

It is physically more realistic to assume that the x-ray spectrum at wavelengths less than 8 Å is produced by thermal processes. We also assume that the line emission contribution is sufficiently small, when compared to the continuum emission, to allow the line emission to be ignored. The predominant source mechanisms for continuum solar x-ray emission are free-free (bremsstrahlung) and free-bound (radiative recombination) electron transitions. Based on equations describing the two emission mechanisms given by Culhane,‡ the dependence on T and λ for each mechanism can be approximated by the proportionalities

$$E_{ff} \approx a(T)g(\lambda_a, \lambda_b)b(\lambda, T) \int N_e^2 dV \quad (\text{B1})$$

and

$$E_{fb} \approx c(T)g'(\lambda_a, \lambda_b)b(\lambda, T) \int N_e^2 dV. \quad (\text{B2})$$

The two mechanisms combined can be represented by

$$E_B \approx [a(T)g(\lambda_a, \lambda_b) + c(T)g'(\lambda_a, \lambda_b)] b(\lambda, T) \int N_e^2 dV, \quad (\text{B3})$$

where

$$b(\lambda, T) = [\lambda^2 \exp(143.89/\lambda T)]^{-1}, \quad (\text{B4})$$

N_e is the electron density in the solar source region, and the integral is evaluated over the volume of the source region. The functions g and g' depend on the band of wavelengths considered, i.e. 0.5 to 3 Å, 1 to 5 Å, or 1 to 8 Å, but don't explicitly depend on wavelength.

From Eq. (7), a conversion constant based on a free-free spectrum, a free-bound spectrum, or a combination of the two can be calculated using

*D.M. Horan, Dissertation submitted to the Catholic University of America, Publication 70-22133, University Microfilms, Inc., 1970.

†D.M. Horan, *Solar Phys.* **21**, 188 (1971).

‡J.L. Culhane, *Monthly Notices Roy. Astron. Soc.* **144**, 375 (1969).

$$K_B(T) = \frac{\int_{\lambda_a}^{\lambda_b} b(\lambda, T) d\lambda}{e\omega \int_{\lambda_1}^{\lambda_2} \epsilon(\lambda) b(\lambda, T) d\lambda} \quad (B5)$$

These constants, which we refer to as bremsstrahlung-type conversion constants, are the same for free-free and free-bound spectra, and combinations of the two because the wavelength dependence is the same for both source mechanisms and only one specific x-ray band is involved. Conversion from fluxes based on the constant-temperature graybody spectrum used for routine processing of the SOLRAD 10 data, $F_{GB}(T_c)$, to fluxes based on a bremsstrahlung-type spectrum at a selected temperature, $F_B(T)$, can be accomplished using

$$F_B(T) = F_{GB}(T_c) \left[\frac{K_B(T)}{K_{GB}(T_c)} \right] = F_{GB}(T_c) G(T). \quad (B6)$$

Values of the ratio G for selected temperatures are given in Table B1 for the 0.5 to 3 Å, 1 to 5 Å, and 1 to 8 Å bands.

Table B1
Temperature-Dependent Conversion Ratios

| Temperature (10^6 K) | $G(T)$ for Experiment Number | | | | |
|----------------------------|------------------------------|--------|-------|-------|-------|
| | 1A | 1B | 2 | 3A | 3B |
| 2 | 0.0215 | 0.0178 | 0.743 | 1.11 | 1.07 |
| 3 | 0.196 | 0.173 | 1.07 | 0.933 | 0.940 |
| 4 | 0.461 | 0.423 | 1.04 | 0.768 | 0.791 |
| 5 | 0.688 | 0.644 | 0.919 | 0.648 | 0.678 |
| 6 | 0.844 | 0.802 | 0.804 | 0.560 | 0.593 |
| 7 | 0.941 | 0.903 | 0.709 | 0.494 | 0.527 |
| 8 | 0.996 | 0.964 | 0.634 | 0.443 | 0.477 |
| 9 | 1.03 | 0.999 | 0.576 | 0.404 | 0.436 |
| 10 | 1.04 | 1.02 | 0.530 | 0.372 | 0.404 |
| 11 | 1.04 | 1.02 | 0.493 | 0.347 | 0.378 |
| 12 | 1.04 | 1.02 | 0.464 | 0.326 | 0.357 |
| 13 | 1.03 | 1.02 | 0.439 | 0.309 | 0.339 |
| 14 | 1.02 | 1.01 | 0.419 | 0.295 | 0.324 |
| 15 | 1.01 | 1.00 | 0.402 | 0.283 | 0.312 |
| 16 | 1.00 | 0.996 | 0.388 | 0.273 | 0.301 |
| 17 | 0.990 | 0.987 | 0.376 | 0.264 | 0.292 |
| 18 | 0.980 | 0.979 | 0.366 | 0.257 | 0.284 |
| 19 | 0.970 | 0.970 | 0.357 | 0.251 | 0.277 |
| 20 | 0.961 | 0.962 | 0.349 | 0.245 | 0.271 |

Based on Eqs. (2) and (B3), the ratio of the currents generated in ionization chambers sensitive to two different bands is given by

$$r_{ij}(T) = \frac{\omega_i A_i [a(T)g_i + c(T)g'_i] \int \epsilon_i(\lambda)b(\lambda, T) d\lambda}{\omega_j A_j [a(T)g_j + c(T)g'_j] \int \epsilon_j(\lambda)b(\lambda, T) d\lambda} \quad (\text{B7})$$

if we assume that the emission measure $\int N_e^2 dV$ is identical for the emission stimulating each detector. This assumption is most valid when the two x-ray bands considered in the ratio are close in wavelength. Note that the relationship expressed in Eq. (B7) is not correct for either free-free or free-bound spectra used alone because the consideration of more than one band prevents the elimination of the functions $a(T)$ and $c(T)$. The equation gives the temperature dependence of the current ratio for the most realistic continuum spectrum — a combination of free-free and free-bound.

The temperature of the emitting source region on the sun can now be obtained by comparing the ratio of currents generated in the i and j detectors to a plot of $r_{ij}(T)$ versus T . However, since the SOLRAD 10 data are available in terms of flux based on a constant-temperature graybody spectrum, it is easier to obtain a ratio of such fluxes than a current ratio. By using Eq. (7), we can convert Eq. (B7) into a ratio of graybody-based fluxes $R_{ij}(T)$, such that

$$R_{ij}(T) = r_{ij}(T) \left[\frac{A_j K^i_{GB}(T_c)}{A_i K^j_{GB}(T_c)} \right]. \quad (\text{B8})$$

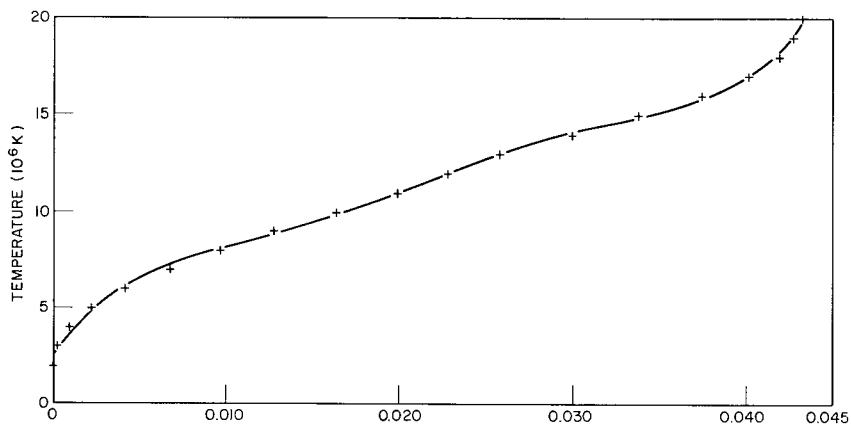
Coefficients of equations in the form

$$T = \sum_{k=0}^5 a_k (R_{ij})^k \quad (\text{B9})$$

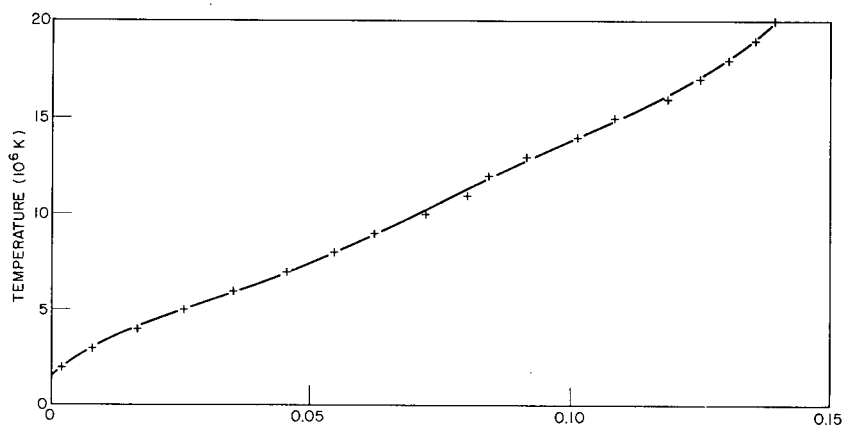
are given in Table B2 for the eight possible flux ratios found from the data of experiments 1 through 3, and Fig. B1 are typical plots of R_{ij} versus T . Temperature T is in units of 10^6 K. The maximum value of T for which Eq. (B9) is valid is given as T_{\max} in Table B2.

Table B2
Coefficients Relating R_{ij} to T

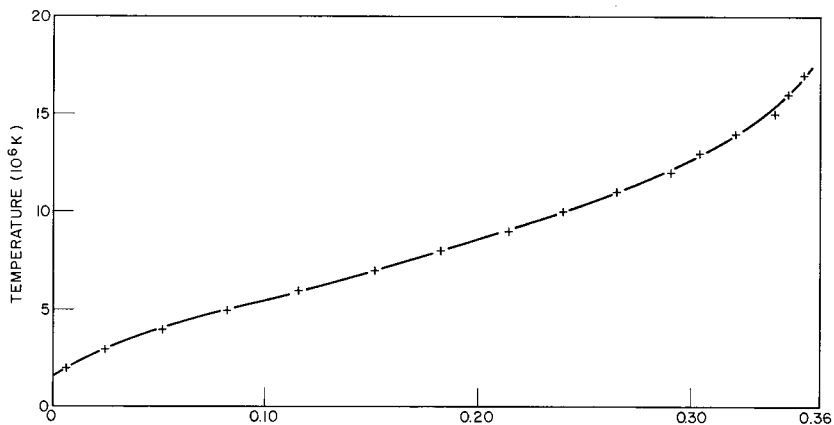
| i/j | a_0 | a_1 | a_2 | a_3 | a_4 | a_5 | T_{\max} |
|-------|-------|---------------------|----------------------|---------------------|----------------------|---------------------|------------|
| 1A/2 | 1.525 | 2.225×10^2 | -5.581×10^3 | 1.059×10^5 | -8.407×10^5 | 2.406×10^6 | 20 |
| 1A/3A | 2.573 | 1.318×10^3 | -1.327×10^5 | 7.541×10^6 | -1.916×10^8 | 1.778×10^9 | 20 |
| 1A/3B | 2.611 | 1.202×10^3 | -1.088×10^5 | 5.560×10^6 | -1.273×10^8 | 1.065×10^9 | 20 |
| 1B/2 | 1.434 | 2.175×10^2 | -5.527×10^3 | 1.054×10^5 | -8.333×10^5 | 2.369×10^6 | 20 |
| 1B/3A | 2.525 | 1.299×10^3 | -1.307×10^5 | 7.427×10^6 | -1.884×10^8 | 1.744×10^9 | 20 |
| 1B/3B | 2.563 | 1.184×10^3 | -1.072×10^5 | 5.481×10^6 | -1.253×10^8 | 1.046×10^9 | 20 |
| 2/3A | 1.495 | 7.659×10^1 | -7.328×10^2 | 5.408×10^3 | -1.832×10^4 | 2.408×10^4 | 17 |
| 2/3B | 1.547 | 7.138×10^1 | -6.166×10^2 | 4.064×10^3 | -1.233×10^4 | 1.453×10^4 | 17 |



(a) Ratio of experiment 1B to experiment 3A.



(b) Ratio of experiment 1A to experiment 2



(c) Ratio of experiment 2 to experiment 3B

Fig. B1 — Typical temperature dependence of the ratios formed from the 0.5 to 3 Å, 1 to 5 Å, and 1 to 8 Å graybody fluxes. The observed flux ratio can be used to determine the electron temperature of a solar region emitting x rays produced by bremsstrahlung or radiative recombination processes.

Therefore, the procedure for converting flux values based on graybody spectra at constant temperatures to flux values based on more realistic free-free plus free-bound spectra at variable temperatures can be summarized as follows:

1. Form the ratio of SOLRAD 10 graybody-based flux values for any two of experiments 1 through 3.
2. Compare the ratio value obtained with the plot of R_{ij} versus T for the selected experiments. This will give the electron temperature T_s of the emitting solar source region.
3. Select the values of $G(T_s)$ from Table B1 for the experiments of interest.
4. Multiply the flux values based on graybody spectra by $G(T_s)$ to obtain flux values based on free-free and free-bound emission from a source region at temperature T_s .

Similar conversions for longer-wavelength experiments have not been attempted because the contribution from line emission cannot be ignored at wavelengths greater than 8 Å.

| Security Classification | | DOCUMENT CONTROL DATA - R & D | |
|---|--|--|--|
| <i>(Security classification of title, body of abstract and indexing annotation must be entered when the overall report is classified)</i> | | | |
| 1. ORIGINATING ACTIVITY <i>(Corporate author)</i> Naval Research Laboratory Washington, D.C. 20390 | | 2a. REPORT SECURITY CLASSIFICATION Unclassified | |
| | | 2b. GROUP | |
| 3. REPORT TITLE THE SOLRAD 10 SATELLITE, EXPLORER 44, 1971-058A | | | |
| 4. DESCRIPTIVE NOTES <i>(Type of report and inclusive dates)</i> An interim report on one phase of the problem; work is continuing. | | | |
| 5. AUTHOR(S) <i>(First name, middle initial, last name)</i> Donald M. Horan and Robert W. Kreplin | | | |
| 6. REPORT DATE July 12, 1972 | 7a. TOTAL NO. OF PAGES 53 | 7b. NO. OF REFS 13 | |
| 8a. CONTRACT OR GRANT NO. NRL Problem A01-20 | 9a. ORIGINATOR'S REPORT NUMBER(S) NRL Report 7408 | | |
| b. PROJECT NO. A3705381-625B-2F00-551-771 | 9b. OTHER REPORT NO(S) <i>(Any other numbers that may be assigned this report)</i> | | |
| c. | | | |
| d. | | | |
| 10. DISTRIBUTION STATEMENT Approved for public release; distribution unlimited. | | | |
| 11. SUPPLEMENTARY NOTES | | 12. SPONSORING MILITARY ACTIVITY Department of the Navy (Naval Air Systems Command), Washington, D.C. | |
| 13. ABSTRACT The Naval Research Laboratory's SOLRAD 10 satellite, also known as Explorer 44 or 1971-058A, was launched on July 8, 1971. The satellite is equipped with sensors to measure solar x-ray and ultraviolet radiation in the following bands: 15 to 150 keV, 0.1 to 1.6 Å, 0.5 to 3 Å, 1 to 5 Å, 1 to 8 Å, 8 to 16 Å, 1 to 20 Å, 44 to 60 Å, 170 to 700 Å, 1080 to 1350 Å, 1225 to 1350 Å, and 1450 to 1600 Å. It also carries an experiment designed to search for radiation in the 0.5 to 15 Å band from nonsolar sources. The satellite is equipped with a data storage system which can accept data from almost all solar experiments with a 1-minute or a 3-minute resolution. The satellite continuously transmits data in real-time at 137.710 MHz. Individual scientists and institutions have been invited through COSPAR to receive and use the data transmitted in real time in their own research programs. To encourage this participation, IRIG channel 7 carries data and status information for almost every solar experiment. The experiment complement aboard SOLRAD 10 is described in detail, and the information needed to convert the telemetered data to solar flux values is provided. | | | |

| 14. KEY WORDS | LINK A | | LINK B | | LINK C | |
|--|--------|----|--------|----|--------|----|
| | ROLE | WT | ROLE | WT | ROLE | WT |
| Satellites Solar satellites SOLRAD 10 Explorer 44 1971-058A Solar x rays Solar ultraviolet radiation | | | | | | |